Circulation Research
JOURNAL OF THE AMERICAN HEART ASSOCIATION

Inhibition of miR-15 Protects Against Cardiac Ischemic Injury

Thomas G. Hullinger, Rusty L. Montgomery, Anita G. Seto, Brent A. Dickinson, Hillary M. Semus, Joshua M. Lynch, Christina M. Dalby, Kathryn Robinson, Christianna Stack, Paul A. Latimer, Joshua M. Hare, Eric N. Olson and Eva van Rooij

Circ Res. 2012;110:71-81; originally published online November 3, 2011;
doi: 10.1161/CIRCRESAHA.111.244442
Circulation Research is published by the American Heart Association, 7272 Greenville Avenue, Dallas, TX 75231

Print ISSN: 0009-7330. Online ISSN: 1524-4571

Inhibition of miR-15 Protects Against Cardiac Ischemic Injury

Thomas G. Hullinger, Rusty L. Montgomery, Anita G. Seto, Brent A. Dickinson, Hillary M. Semus, Joshua M. Lynch, Christina M. Dalby, Kathryn Robinson, Christianna Stack, Paul A. Latimer, Joshua M. Hare, Eric N. Olson, Eva van Rooij

Rationale: **Myocardial infarction (MI) is a leading cause of death worldwide. Because endogenous cardiac repair mechanisms are not sufficient for meaningful tissue regeneration, MI results in loss of cardiac tissue and detrimental remodeling events. MicroRNAs (miRNAs) are small, noncoding RNAs that regulate gene expression in a sequence dependent manner. Our previous data indicate that miRNAs are dysregulated in response to ischemic injury of the heart and actively contribute to cardiac remodeling after MI.**

Objective: **This study was designed to determine whether miRNAs are dysregulated on ischemic damage in porcine cardiac tissues and whether locked nucleic acid (LNA)-modified anti-miR chemistries can target cardiac expressed miRNAs to therapeutically inhibit miR-15 on ischemic injury.**

Methods and Results: **Our data indicate that the miR-15 family, which includes 6 closely related miRNAs, is regulated in the infarcted region of the heart in response to ischemia-reperfusion injury in mice and pigs. LNA-modified chemistries can effectively silence miR-15 family members in vitro and render cardiomyocytes resistant to hypoxia-induced cardiomyocyte cell death. Correspondingly, systemic delivery of miR-15 anti-miRs dose-dependently represses miR-15 in cardiac tissue of both mice and pigs, whereas therapeutic targeting of miR-15 in mice reduces infarct size and cardiac remodeling and enhances cardiac function in response to MI.**

Conclusions: **Oligonucleotide-based therapies using LNA-modified chemistries for modulating cardiac miRNAs in the setting of heart disease are efficacious and validate miR-15 as a potential therapeutic target for the manipulation of cardiac remodeling and function in the setting of ischemic injury. (*Circ Res*. 2012;110:71-81.)**

Key Words: microRNA ■ ischemia reperfusion ■ miR-15 family ■ anti-miR therapy

Ischemic heart disease can lead to congestive heart failure, which is the leading cause of death worldwide.[1] Ischemic heart disease is induced by an insufficient oxygen supply to the myocardium, typically due to coronary artery disease or myocardial infarction (MI). During an MI, occlusion of coronary vessels impedes a sufficient oxygen supply to the heart muscle and the resulting hypoxia results in loss of viable cardiac tissue, which often correlates with impairment of cardiac contractility. In response to ischemic injury, the nonischemic myocardium displays signs of secondary remodeling, such as interstitial fibrosis and hypertrophy of cardiac myocytes, which further diminish pump function and increase susceptibility to arrhythmias. Currently, the most effective strategy for reducing the size of a myocardial infarct and improving the clinical outcome after an acute MI is early myocardial reperfusion by either thrombolytic therapy or primary percutaneous coronary intervention. Cardiac cell therapy as a means of regenerating the infarcted heart has made substantial progress. In recent years, randomized, controlled clinical trials have demonstrated that cell therapy can improve cardiac function in patients after MI. However, current limitations for cell therapy are the low rates of cell engraftment after intracoronary delivery and poor cell survival after intramyocardial injections.[2]

Data from us and others have indicated that microRNAs (miRNAs) play important roles during different forms of heart disease. Previously, we showed that miRNAs are dysregulated in response to MI and contribute to the cardiac remodeling process induced by infarction.[3] MiRNAs are short, 21- to 25-nucleotide noncoding RNAs that modulate gene expression by base pairing with the 3′

Original received March 9, 2011; revision received October 19, 2011; accepted October 20, 2011. In September 2011, the average time from submission to first decision for all original research papers submitted to *Circulation Research* was 16 days.

From miRagen Therapeutics, Inc, Boulder, CO (T.G.H., R.L.M., B.A.D., H.H.S., J.M.L., C.M.D., K.R., C.S., P.A.L.); University of Miami Miller School of Medicine, Interdisciplinary Stem Cell Institute, Miami, FL (J.M.H.); and the Department of Molecular Biology, University of Texas Southwestern Medical Center, Dallas, TX (E.N.O.).

This manuscript was sent to Ali J. Marian, Consulting Editor, for review by expert referees, editorial decision, and final disposition.

Correspondence to Eva van Rooij, miRagen Therapeutics, Inc, 6200 Lookout Rd, Boulder, CO 80301. E-mail evanrooij@miragenrx.com

Circulation Research **is available at http://circres.ahajournals.org** **DOI: 10.1161/CIRCRESAHA.111.244442**

Non-standard Abbreviations and Acronyms	
ATP	adenosine triphosphate
L/D 15b	LNA/DNA 16-mer anti–miR-15b
LNA	locked nucleic acid
MI	myocardial infarction
miR/miRNA	microRNA
tiny 15b	LNA 8-mer anti–miR-15b
2′ ome	2′-O-methyl

untranslated regions of mRNAs, and inducing mRNA degradation or translational inhibition of the target. Nucleotides 2–8 of the 5′ end of the miRNA, called the "seed sequence," are especially important for mRNA target interaction. Interestingly, most miRNAs belong to families of closely related miRNAs with homologous seed sequences while differing in their 3 portion.[4] Because the seed region is conserved, miRNA family members can presumably regulate overlapping target genes.

We show the dynamic pattern of miRNA expression in a porcine model of ischemic damage both short term and long term after injury. Especially intriguing is the upregulation of a family of miRNAs, called the miR-15 family, in the infarct region on ischemic injury. The miR-15 family consists of multiple miRNAs (miR-15a, miR-15b, miR-16–1, miR-16–2, miR-195, and miR-497) and is consistently found to be upregulated in different settings of heart disease (reviewed in Small et al[5]). Although the cardiac functions of this miRNA family have not been previously defined in vivo, these miRNAs are predicted to influence cardiomyocyte cell survival by regulating the expression of several prosurvival proteins, including Arl2 and Bcl2.[6,7]

The use of chemically modified, single-stranded oligonucleotides has been shown to be effective in inactivating specific miRNAs in vivo through complementary base pairing.[8–13] Our data show that LNA-modified anti-miR chemistries can effectively silence miR-15 family members in vitro and render cardiomyocytes resistant to hypoxia-induced cardiomyocyte cell death. Correspondingly, systemic delivery of a miR-15 anti-miR dose-dependently represses miR-15 family members in both murine and porcine cardiac tissue, whereas therapeutic dosing of anti-miR chemistries targeting miR-15 in mice reduces infarct size, inhibits cardiac remodeling, and enhances cardiac function in response to ischemic damage. These studies represent an important step toward optimization of oligonucleotide-based therapies for modulation of cardiac miRNAs, and validate miR-15 as a therapeutic target for the manipulation of cardiac remodeling and function in the settings of ischemic heart disease.

Methods

An expanded Methods section describing all procedures and protocols is available in the Online Data Supplement at http://circres.ahajournals.org.

Animals

All animal studies were reviewed and approved by the Animal Care and Use Committee (IACUC) at miRagen Therapeutics, Inc (murine studies) or the University of Miami IACUC (porcine ischemia-reperfusion study) and comply with Federal and State guidelines concerning the use of animals in research and teaching as defined by The Guide For the Care and Use of Laboratory Animals (NIH Publication No. 80–23, revised 1985). The porcine dose-ranging studies were done by AccelLAB (Boisbriand, Canada), which is accredited by the Canadian Council on Animal Care (CCAC) and complies to IACUC requirements and to those of the Guide for the Care and Use of Laboratory Animals of the United States Department of Agriculture (USDA).

Ischemia-Reperfusion Surgery

Female Yorkshire pigs (3 months of age; weight, 25–30 kg; n=4) were subjected to MI by inflation of a coronary angioplasty balloon in the left anterior descending artery for 60 minutes, followed by reperfusion. Ischemia-reperfusion in male C57Bl6 adult mice (8–10 weeks of age) was induced by 75 minutes of left coronary artery occlusion followed by reperfusion for either 24 hours or 2 weeks as described previously.[14] More details can be found in the on-line Data Supplement.

Microarray for miRNAs and mRNAs

Microarray analysis was performed on total RNA, using a service provider (LC Sciences, Houston, TX) as described previously.[3] Detailed description can be found in the on-line Data Supplement.

Real-Time PCR

Total RNA from cardiac tissue was isolated using Trizol (Invitrogen). RT-PCR with random hexamer primers (Invitrogen) was performed on RNA samples, after which the expression of a subset of genes was analyzed by either a regular or quantitative real-time PCR, using gene-specific primers or Taqman probes purchased from ABI. For quantitative real-time PCR, a pool of synthetic microRNAs was used to generate a standard curve. Manufacturer's instructions were followed for the standard curve starting concentration and subsequent serial dilution (Ambion miRvana reference library).

Cell Culture and Luciferase Assay

HeLa cells and neonatal cardiomyocytes were cultured as described previously.[15] Transfection experiments in HeLa cells for luciferase assays were performed according to the manufacturer's instructions. More details can be found in the on-line Data Supplement.

Model of Hypoxia and Reoxygenation

Immediately after transfection, cells were placed in either a low oxygen atmosphere or normoxic conditions. To induce hypoxia, cells were incubated in a humidified environment at 37°C in a 3-gas hypoxic chamber maintained at 5% CO_2 and 0.2%O_2 (oxygen expelled by nitrogen) for 72 hours. Normoxic cells were maintained in 2% serum in a normoxic incubator (21% O_2, 5% CO_2, 37°C). After 72 hours of hypoxia, cells were exposed to 3 hours of reoxygenation under normoxic conditions and in media containing 2% serum.

Myocyte Survival Assays

After exposure to normoxia, hypoxia, or hypoxia plus reoxygenation for the indicated periods of time, several detection methods were used to determine apopotosis/cell survival. A detailed description can be found in the online Data Supplement.

Intravenous Delivery of LNA-Modified Anti-miRs

The LNA–anti-miR oligonucleotides were synthesized at miRagen Therapeutics, Inc as unconjugated and fully phosphorothiolated oligonucleotides. The perfectly matching LNA–anti-miR oligonucleotide was complementary to the 5′ region of the mature miR-15b

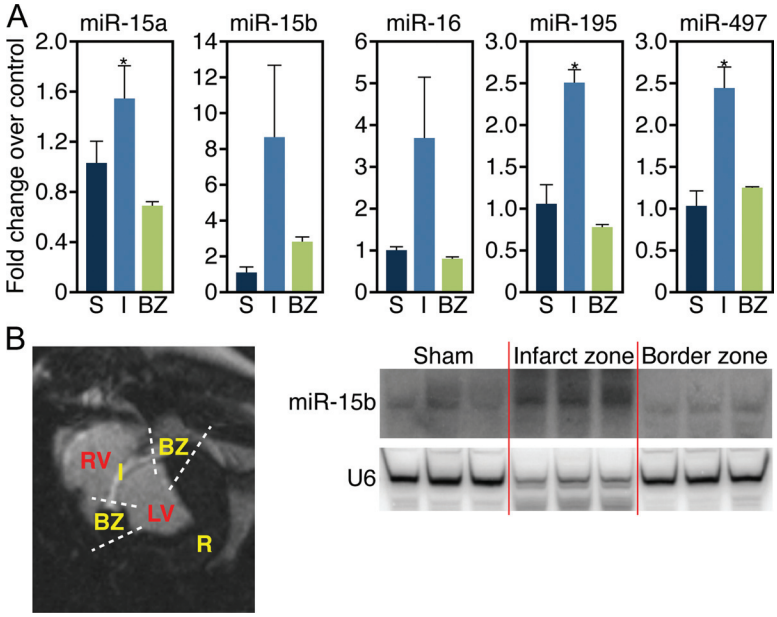

Figure 1. miR-15 family is upregulated in the infarcted region of porcine cardiac tissue in response to ischemic injury. A, Real-time PCR analysis indicates that the miR-15 family is upregulated in the infarct zone in porcine cardiac tissue 24 hours after ischemia-reperfusion. miR-15a, miR-195, and miR-497, *$P<0.05$ versus border zone; miR-15b, $P=0.13$; miR-195, $P=0.09$ (ANOVA); n=3 per group. S indicates sham; LV, left ventricle; RV, right ventricle; I, infarct; BZ, border zone. **B**, MRI cross-sectional image of porcine heart demonstrating I, BZ, normally perfused remote region (R), LV, and RV. Northern blot analysis of porcine cardiac tissue from these areas indicates an upregulation of miR-15b specifically in the infarcted region 24 hours after ischemia-reperfusion.

sequence (either nucleotides 2–17 or 2–9). The LNA control oligonucleotide consisted of a sequence directed against a *Caenorhabditis elegans* miRNA that is not expressed in mammals. Eight- to 10-week-old C57BL/6 mice or young pigs were injected intravenously with the indicated doses of anti-miR, universal control, or a comparable volume of saline, after which tissues were collected at the indicated time points.

Northern Blot Analysis

Total RNA was isolated from porcine or mouse cardiac tissue samples by using Trizol reagent (Gibco/BRL). Northern blot analysis for the experiments in which LNA-modified anti-miR chemistries were used were performed on nondenaturing gels to show the heteroduplex formation between the LNA and mature miRNAs, as described previously.[9]

Tissue and Plasma Distribution Assay

Levels of anti-miRs in plasma or tissues were measured using a hybridization assay method to detect the L/D 15b. A competition assay was used to detect tiny 15b. Detailed descriptions can be found in the online Data Supplement.

Infarct Size Determination

After 24 hours of reperfusion, the mice were anesthetized and the left main coronary artery ligation site was identified and religated. Evans Blue dye (1.2 mL of a 2.0% solution, Sigma) was injected through a carotid artery catheter into the coronary circulation to delineate the ischemic zone from the nonischemic zone. Triphenyltetrazolium chloride (Sigma) was used to demarcate the viable and nonviable myocardium within the ischemic zone. More details can be found in the online Data Supplement.

Echocardiography

Cardiac function and heart dimensions were evaluated by 2-dimensional echocardiography in mice sedated with 5% isoflurane using a Visual Sonics Vevo 770 Ultrasound (Visual Sonics, Toronto, Canada), as described.[16] More details can be found in the online Data Supplement.

Statistical Analysis

One-way ANOVA and Newman-Keuls multiple comparison posttest or a *t* test were used to determine significance. $P<0.05$ was considered statistically significant.

Results

miRNAs Are Dynamically Regulated in Response to Ischemia-Reperfusion Injury

Based on recent data showing miRNA dysregulation during cardiac remodeling, we set out to examine whether miRNAs are also involved in ischemia-reperfusion injury of the porcine heart. To this end, we performed miRNA microarray analysis on porcine cardiac samples both 2 and 8 weeks after ischemia-reperfusion injury and profiled miRNA expression in the infarct and border zone regions post-MI compared with control tissue from sham-operated animals. The data showed a distinct miRNA expression signature and indicated that miRNAs are dynamically regulated in different regions of the porcine heart during post-MI remodeling, which could be confirmed by miRNA-specific real-time PCR analysis (Supplemental Tables I and II and Supplemental Figure I, A). Although many of the regulated miRNAs have previously been implicated in cardiac disease, several dysregulated miRNAs had so far not been connected to cardiac disease (Supplemental Tables I and II).

Because infarct healing is a dynamic process involving specific regional and temporal changes in cardiomyocyte hypertrophy, apoptosis, and fibrosis, we next assessed the regulation of these miRNAs more acutely after MI. Real-time analysis confirmed the regulation of specific miRNAs in the infarcted and borderzone region 24 hours after the ischemic injury (Supplemental Figure IB). Interestingly, all members of the miR-15 family (miR-15a, -15b, -16, -195, and -497) were found to be upregulated in the infarcted region 24 hours after ischemic injury in the porcine MI model, as assessed by both real-time PCR analysis and Northern blot (Figure 1A and 1B). Although the signal for the loading control was reduced in the infarcted region (U6), probably because of the loss of viable cells, there was a significant increase in miR-15b. Of the miR-15 family, only miR-15b was still elevated

several weeks after infarction in both pigs (Supplemental Figure I, A) and mice.[3]

Anti–miR-Mediated miR-15b Inhibition In Vitro

The miR-15 family members are expressed as 3 bicistronic clusters (Supplemental Figure II), and all contain a comparable seed sequence (Figure 2A). Although all 3 clusters are expressed in the heart, miR-16 is most abundant and miR-497 has the lowest expression, as determined by absolute copy number per cell in vivo (≈10 000 copies versus 300 copies per cardiac cell) (Supplemental Figure III, A). In vitro analysis of the different miR-15 family members indicates a comparable relative abundance for the different members in fibroblasts and myocytes, albeit at a much lower level than they are detected at in vivo (Supplemental Figure III, B). Because the miR-15 family has been implicated in apoptosis,[17] we hypothesized that elevated levels of miR-15 family members in response to ischemic injury might contribute to a decrease in viable cardiomyocytes. To develop an efficient approach for miR-15 targeting in vivo, we evaluated the in vitro potency of 2 LNA-modified DNA oligonucleotide anti-miRs (either 16 or 8 nucleotides in length), and compared it with a cholesterol-modified antagomir-15b (Figure 2A). The 16mer anti-miR is an LNA/DNA anti-miR complementary to the 5′ end of miR-15b (L/D 15b). As a consequence of the high binding affinity for LNA-containing antisense oligonucleotides, biological activity is often attained with shorter LNA oligonucleotides.[18] We also tested an 8-mer LNA–anti-miR complementary to the seed region of the miR-15 family, which would be predicted to target all family members (tiny 15b). In parallel, we also tested an antagomir against miR-15b, which is the full-length complementary reverse sequence of miR-15b in which all nucleosides are 2′-O-Methyl (Ome) modified with the 5′ terminal two and 3′ terminal 4 bases containing a phosphorothioate internucleoside bond and a 3′ cholesterol attached through a hydroxyprolinol linker (Figure 2A).

To test for functional activity, we generated luciferase reporters harboring a perfect binding site for the different miR-15 members (miR-15b, -16, and -195), such that inhibition of endogenous miR-15 members in HeLa cells would lead to an increase in luciferase activity. We focused on these particular family members because they appeared to be most highly regulated in vivo (Figure 1A). Luciferase reporter assays indicated a dose-responsive derepression of the miR-15b luciferase reporter for all 3 oligonucleotide chemistries tested, with the L/D 15b being most efficacious and the antagomir-15b showing the least activity. As expected, based on sequence composition, tiny 15b also repressed miR-16 and -195 activity, whereas the L/D 15b preferentially inhibited miR-15b (Figure 2B). These data correlate with the knockdown efficiency for the miR-15 family members in cardiomyocytes, as measured by real-time PCR analysis (Figure 2C). Subsequent mRNA analysis of ADP-ribosylation factor–like protein 2 (Arl2), a defined miR-15 target, indicated a dose-dependent increase in response to increasing inhibition of the miR-15 family with tiny 15b in cardiomyocytes,

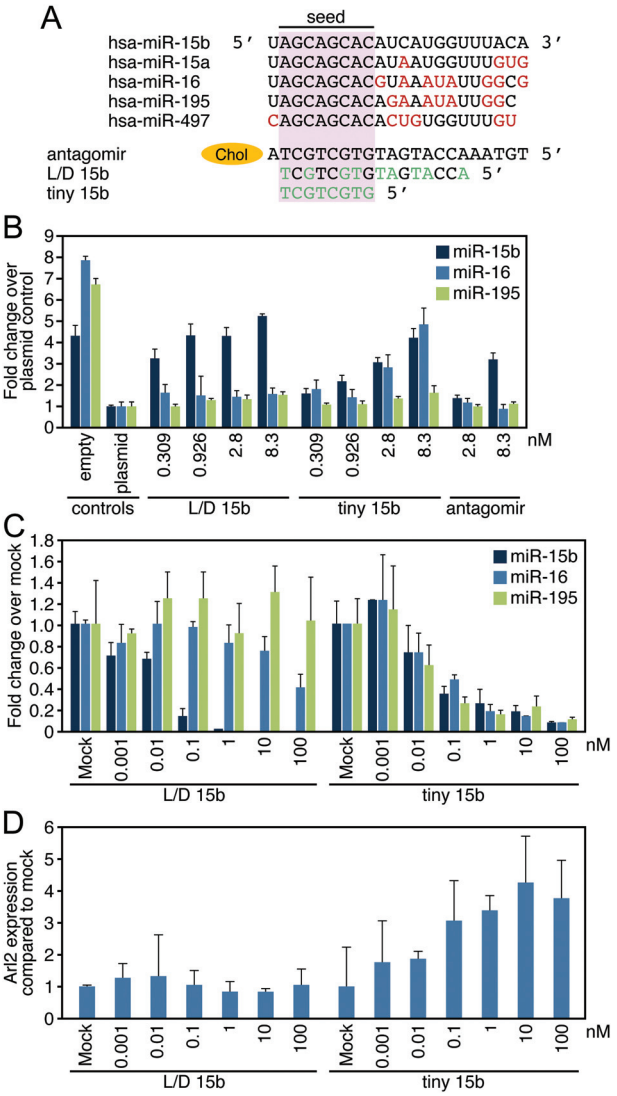

Figure 2. Anti-miR–mediated silencing of miR-15 family members in vitro. A, miR-15 family sequences and anti-miR designs. Antagomir 15b is directed against miR-15b, and contains the full length complementary reverse sequence of the mature miRNA in which all nucleosides are 2′-Ome modified with two 5′ terminal and four 3′ terminal bases containing a phosphorothioate internucleoside bond and a 3′ cholesterol (chol) attached through a hydroxyprolinol linker. The 16-mer anti-miR is an unconjugated LNA/DNA anti-miR complementary to the 5′ end of miR-15b (L/D 15b), whereas the 8-mer LNA–anti-miR is complementary to the seed region of the miR-15 family (tiny 15b). The LNA-modified chemistries are fully phosphorothioated (green indicates LNA). **B**, Luciferase assays in Hela cells using reporters harboring a perfect binding site for the different miR-15 members (miR-15b, -16, and -195) indicated a dose-responsive derepression of the miR-15b luciferase reporter for all 3 oligonucleotide chemistries tested, with the L/D 15b being most efficacious and the antagomir-15b showing the least activity. As expected based on sequence composition, tiny 15b also represses miR-16 and -195 activity, whereas the L/D 15b preferentially inhibits miR-15b. **C**, Real-time PCR analysis in cardiomyocytes shows that L/D 15b potently inhibits miR-15b, whereas tiny 15b inhibits multiple family members (empty indicates plasmid without target site; plasmid, plasmid with target site). **D**, Real-time PCR analysis for Arl2, a defined miR-15 target, shows a dose-dependent derepression in response to increasing doses of tiny 15b, whereas this response is absent in the L/D treated cells. **B** through **D** show average results for 3 independent experiments.

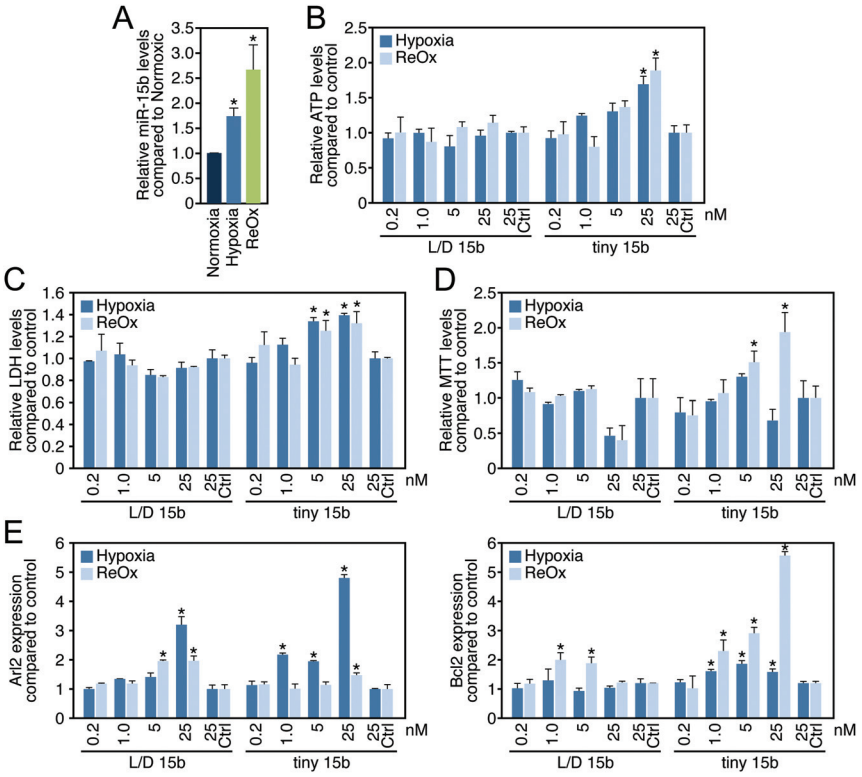

Figure 3. miR-15 inhibition increases cardiomyocyte survival under hypoxic conditions. A, miR-15b levels increase in cardiomyocytes in response to hypoxia, which is further enhanced by subsequent reoxygenation (*$P<0.05$ versus normoxia by ANOVA). **B**, Cardiomyocyte survival, as determined by relative ATP levels, increases dose-dependently in response to tiny 15b compared with control, whereas this effect is absent for L/D 15b (Ctrl indicates control oligonucleotide, *$P<0.05$ versus respective control by ANOVA). **C**, Measuring numbers of cells through total cytoplasmic lactate dehydrogenase indicates that tiny 15b dose-dependently increases cell viability during hypoxia and hypoxia/reoxygenation. (Ctrl indicates control oligonucleotide,*$P<0.05$ versus respective control by ANOVA). **D**, Using the MTT assay as a measure of cell viability shows that tiny 15b dose-dependently increases cell viability compared with control treatment, especially under conditions of hypoxia/reoxygenation (Ctrl indicates control oligonucleotide, *$P<0.05$ versus respective control by ANOVA). **E**, Real-time PCR analysis indicates that both L/D 15b and tiny 15b dose-dependently increase the miR-15 target Arl2 compared with control; however, this effect is most pronounced after tiny 15b treatment under hypoxic conditions. Real-time PCR analysis for Bcl2 shows a moderate increase after L/D 15b treatment during reoxygenation; however, this effect is significantly more pronounced in response to tiny 15b treatment (Ctrl indicates control oligonucleotide, *$P<0.05$ versus respective control by ANOVA). Figure represents average data from 3 independent experiments.

whereas this response was absent after treatment with L/D 15b (Figure 2D).

miR-15 Inhibition Increases Cardiomyocyte Viability in Response to Hypoxia

Because miR-15 is upregulated in vivo in response to ischemic stress and potentially contributes to cardiomyocyte survival, we aimed to determine the effect of miR-15 in hypoxic myocytes and fibroblasts in culture. We were able to verify the conditions of hypoxia and hypoxia/reoxygenation by measuring creatine kinase levels (Supplemental Figure IV, A) and miR-210 and VEGFa expression in both cardiomyocytes and fibroblasts, all known to show an increase in expression in response to hypoxic injury (Supplemental Figure IV, B).To examine the effect of miR-15 inhibition on cell survival/viability, we made use of the adenosine triphosphate (ATP)-based cytotoxicity assay, which utilizes the bioluminescent measurement of ATP present in metabolically active cells to assess cell viability (Supplemental Figure IV, C).[19,20,21] Compared with normoxic myocytes (norm), miR-15b was induced in cardiomyocytes under hypoxic conditions (hyp), which was further enhanced by subsequent reoxygenation (reox) (Figure 3A). Both during hypoxia and hypoxia with subsequent reoxygenation, we achieved efficient knockdown for both L/D 15b and tiny 15b compared with control transfected cells as determined by real-time PCR analysis (Supplemental Figure IV, D).

Our data show that tiny 15b in cardiomyocytes dose-dependently increases cardiomyocyte cell survival both under hypoxic conditions and after hypoxia with subsequent reoxygenation as indicated by an increase in relative ATP levels (Figure 3B), which is absent in fibroblasts under the same conditions (Supplemental Figure IV, E). Additionally, we measured cell viability during hypoxia and reoxygenation through 2 enzyme release assays. One is the LDH assay, which is a means of measuring number of cells through total cytoplasmic lactate dehydrogenase, and the second assay is the MTT assay, which is also a measure of cell health and viability. Both assays show that tiny 15b increases cells viability under hypoxic conditions in vitro (Figure 3C and 3D). The increase in myocyte survival corresponded to a dose-dependent increased in Arl2 during hypoxia and an increase in Bcl2 during hypoxia, which became even more pronounced during reoxygenation (Figure 3E). Whereas L/D 15b also increased the expression of Arl2, there was only a moderate effect on Bcl2 expression, making it tempting to speculate that the additional increase in Bcl2 is required to establish the protective effects on cardiomyocytes during hypoxia as seen for tiny 15b.

Silencing of miR-15 Family Members in Murine Cardiac Tissue by LNA-Modified Anti-miRs

Next, we examined whether LNA–anti-miRs were able to silence cardiac miR-15 family members in vivo. Because the final goal would be to inhibit miR-15 during a stress-induced increase of miR-15b, mice received angiotensin II 3 days before anti-miR treatment to elevate cardiac miR-15b levels (Supplemental Figure V, A). Sin-

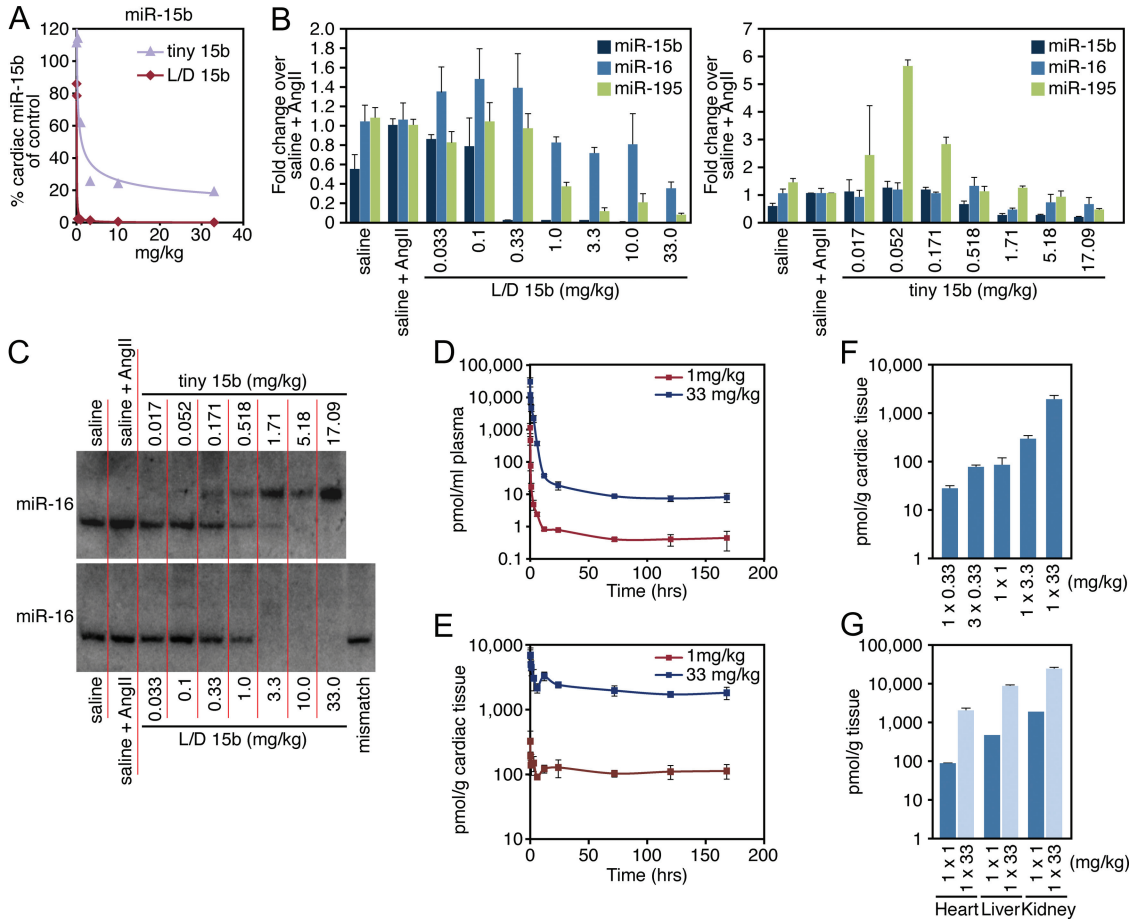

Figure 4. Cardiac silencing of miR-15 in mice using an LNA-modified anti-miR. A, Real-time PCR analysis for miR-15b 1 week after intravenous administration of increasing doses of L/D 15b or equalmolar amounts of tiny 15b indicates potent silencing of cardiac miR-15b. **B**, Real-time PCR analysis 1 week after systemic administration of either L/D 15b or equal molar amounts of tiny 15b shows effective knockdown for multiple miR-15 family members in response to angiotensin II treatment. As expected based on sequence composition, tiny 15b also represses miR-16 and -195 activity, whereas L/D 15b preferentially inhibits miR-15b. **C**, Northern blotting confirms a dose-dependent cardiac silencing of miR-16. The detectable upshift of miR-16 in the presence of tiny 15b reflects the formation of a stable heteroduplex between miR-16 and the LNA–anti-miR. Inhibition of miR-16 in response to tiny 15b indicates a more pronounced inhibition by Northern analysis, because the real-time PCR procedure disrupts the binding between the anti-miR and tiny 15b, presenting an underrepresentation of anti–miR-miRNA interaction. **D**, Plasma detection of L/D 15b shows a rapid (6–12 hours) elimination phase, after which small amounts of anti-miR remain detectable in the plasma for at least 7 days in a dose-dependent manner. **E**, L/D 15b detection in cardiac tissues indicates a dose-dependent presence of anti-miR, which remains fairly stable between days 1 and 7. **F**, The detection of L/D 15b in cardiac tissue 1 week after administration is dose-dependent. **G**, Tissue detection in heart, liver, and kidney shows that considerable amounts of L/D 15b target the liver and kidney. Data represent the average of n=4 per group.

gle intravenous injections of doses ranging from 0.033 mg/kg to 33 mg/kg of L/D 15b or equal molar amounts of tiny 15b through the tail vein resulted in dose-dependent repression of cardiac miR-15b 1 week after injection, as determined by real-time PCR analysis. The L/D 15b anti-miR showed the highest efficiency in antagonizing miR-15b (Figure 4A and Supplemental Figure V, B). Real-time PCR analysis for additional family members showed that 1 week after administration the targeting efficiency of tiny 15b was more distributed over the family with the exception of miR-15a, whereas the truncated L/D 15b anti-miR preferentially targeted miR-15b (Figure 4B and Supplemental Figure V, B). Currently, we have no explanation for the detected increase in miR-195 in response to the low dose of tiny 15b. The efficient knockdown of miR-15 family members was confirmed by Northern blot analysis for miR-16 (Figure 4C). Notably, we observed an upshift of miR-16 in the presence of tiny 15b when we used an LNA-probe that spanned the entire length of the miR-16 sequence. This upshift reflects the formation of a stable heteroduplex between miR-16 and the LNA anti-miR. Although Northern analysis shows efficient inhibition of miR-16 with the L/D 15b anti-miR, this oligonucleotide covers too much of the miRNA for the probe to bind and showed the anti–miR-miRNA heteroduplex. The injected animals showed no evidence of LNA-associated toxicities or histopathologic abnormalities in the heart, liver, or kidneys (data not shown).

Biodistribution data for the L/D 15b anti-miR were collected using a sandwich hybridization assay, using 2′Ome modified capture and detection probe. Within 6 to 12 hours after intravenous delivery, the majority of the

Table. Outline of Porcine Anti-miR Studies

Anti-miR	Dose, mg/kg	Killed	No. of Animals
Saline	. . .	Day 4	3
L/D 15b	0.033	Day 4	3
L/D 15b	0.1	Day 4	3
L/D 15b	0.33	Day 4	3
L/D 15b	1	Day 4	3
L/D 15b	3.3	Day 4	3
Saline	. . .	Day 4	3
Tiny 15b	0.518 (1)	Days 1 and 4	3 and 3
Tiny 15b	1.71 (3.3)	Days 1 and 4	3 and 3
Tiny 15b	5.18 (10)	Days 1 and 4	3 and 3

Tiny 15b was dosed at equal molar amounts of 1, 3.3, and 10 mg/kg of L/D 15b.

anti-miR cleared from the plasma for both the 1 and 33 mg/kg doses but remained detectable until 168 hours (1 week) after injection (Figure 4D). Cardiac detection of the anti-miR indicated high levels of anti-miR for the first 6–12 hours (probably because of the level of anti-miR in the circulation), after which substantial amounts remained present in the heart at a relatively steady level of detection (Figure 4E). Cardiac detection 1 week after administration was dose-dependent (Figure 4F), whereas higher levels of anti-miR could be detected in liver and kidney (Figure 4G). Using a competition assay, comparable data analysis was performed on the tiny 15b treated samples, which indicated equivalent biodistribution data for tiny 15b (Supplemental Figure VI).

To determine whether the route of administration influenced the inhibitory capacity of the anti-miRs, we compared intravenous, intraperitoneal, subcutaneous, and gavage administration side-by-side. These studies showed comparable inhibition 4 days after a single intravenous, intraperitoneal, or subcutaneous administration of both L/D 15b and tiny 15b. Gavage delivery also resulted in cardiac inhibition of miR-15b, albeit with a lesser efficiency (Supplemental Figure VII).

In Vivo Silencing of miR-15 in Porcine Cardiac Tissue

To verify whether we could extrapolate the murine knockdown data of the LNA-modified anti-miRs to a larger animal model, we delivered increasing doses of L/D 15b or tiny 15b to pigs intravenously through the ear vein (Table). Four days after injection, both real-time PCR and Northern blot analysis on biopsies taken from the left ventricle indicated that 1.0 mg/kg of L/D 15b was sufficient to inhibit miR-15b in the porcine heart by greater than 90% (Figure 5A and 5B). Northern blot showed that L/D 15b preferentially inhibited miR-15b (Figure 5B), whereas tiny 15b inhibited miR-15b and miR-16 as potently (Figure 5C and 5D), just as was seen in vitro and in mice. Parallel real-time PCR analysis on the left ventricle (LV), septum (Sep) or right ventricle (RV), indicated that the knockdown efficiency was comparable in different portions of the heart (Supplemental Figure VIII). Both 1 and 4 days after intravenous delivery,

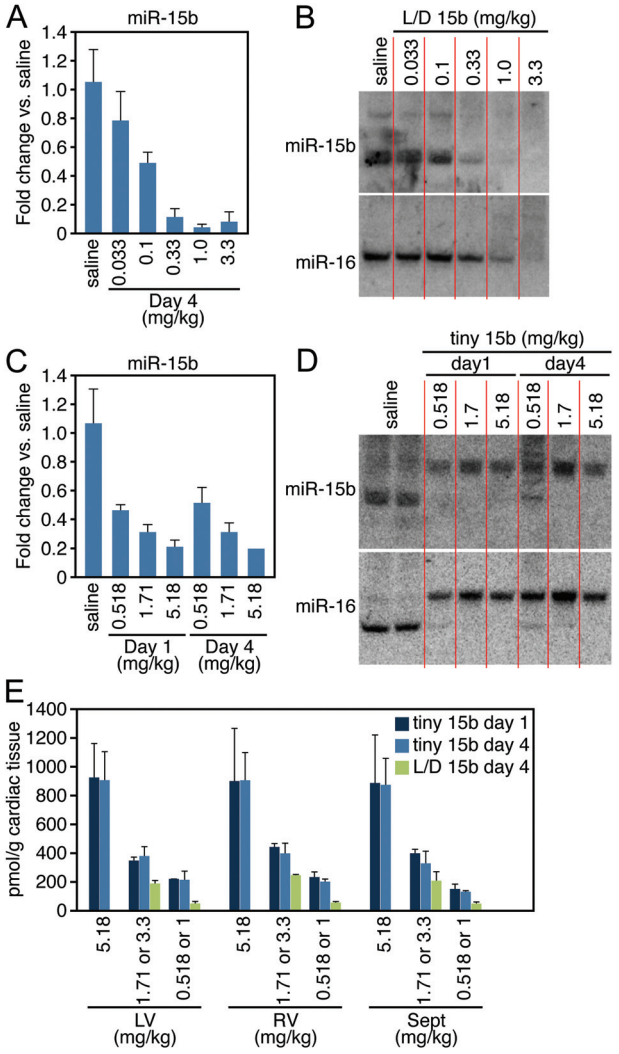

Figure 5. miR-15 inhibition in porcine cardiac tissue. A, Real-time PCR analysis 4 days after intravenous administration of increasing doses of L/D 15b indicates potent silencing of cardiac miR-15b. **B**, Northern blotting confirms a dose-dependent cardiac silencing of miR-15b and miR-16 in porcine cardiac tissue 4 days after dosing. L/D 15b preferentially target miR-15b. **C**, Real-time PCR analysis both 1 and 4 days after intravenous administration of increasing doses of tiny 15b indicates potent silencing of cardiac miR-15b. **D**, Northern blotting confirms a dose-dependent cardiac silencing of miR-15b and miR-16 in porcine cardiac tissue in response to tiny 15b treatment. The observed upshift reflects the formation of a stable heteroduplex between the mature miRNAs and the LNA–anti-miR. **E**, Cardiac detection of L/D 15b and tiny 15b shows a relatively equal distribution of the anti-miR across the heart that is dose-responsive for both anti-miRs, with no differences in detectable amount of anti-miR between days 1 and 4 after tiny 15b administration. When 2 doses are indicated, the first dose is tiny 15b and second dose is L/D 15b. LV indicates left ventricle; RV, right ventricle; and Sept, interventricular septum. Data represent the average of n=3 per group.

tiny 15b induced efficient silencing of miR-15 members, as indicated by both real-time PCR and Northern blotting (Figure 5C and 5D).

Compared with the Northern blot data, real-time PCR appears to underestimate miR-15b inhibition, probably the result of a disruption of the anti–miR-miRNA binding during the PCR procedure. Tissue distribution data for

both chemistries in different portions of the heart indicate comparable dose-dependent detection at days 1 and 4 for tiny 15b in LV, RV, and Sep, which corresponds well to the detected quantities for L/D 15b at day 4 when dosed with equal molar amounts (Figure 5E). The plasma and tissue distribution data look identical to the murine data when dosed with a comparable amount of anti-miR (data not shown).

All mice tolerated the anti-miR or control oligo well and exhibited normal behavior, as determined by activity level and grooming throughout the study. Compared with saline, anti–miR-15b did not induce changes in body or tissue weights up to 6 weeks after dosing (data not shown). Both L/D 15b and tiny 15b did not change serum levels of the alanine aminotransferase and aspartate aminotransferase liver enzymes in pigs (Supplementary Figure IX, A), nor were there any observable abnormalities histologically, suggesting that the oligonucleotides do not induce any overt toxicities (Supplemental Figure IX, B).

miR-15 Inhibition Protects Against Ischemia-Induced Injury

To test the functional relevance of miR-15 inhibition during ischemia-reperfusion injury, we injected mice at the onset of reperfusion after 75 minutes of ischemia intravenously with tiny 15b, control oligo, or vehicle control (saline). The extent of myocardial infarction was determined 24 hours after reperfusion and indicated that treatment with tiny 15b during reperfusion resulted in a significant decrease in infarct size compared with either saline or control oligo, whereas there were no observable differences in area at risk (Figure 6A and 6B). Real-time PCR analysis on the ischemic region of the heart showed that miR-15b was induced after an ischemic event and that 0.5 mg/kg of tiny 15b resulted in a 72% reduction of cardiac miR-15b levels in the ischemic region 24 hours after reperfusion (Figure 6C). Hemodynamic analysis 24 hours after ischemia shows a significant increase in LV end-diastolic pressure, which was absent in response to tiny 15b treatment (Figure 6D). Microarray analysis on saline, tiny 15b, or control injected animals after ischemia-reperfusion indicates an overrepresentation of negative regulators of cell death upregulated in the tiny 15b–treated group (Figure 6E and Supplemental Tables III and IV). Although the intersample variation between the groups was quite large, 23 TargetScan-predicted targets of the miR-15 family were found by microarray analysis to be derepressed with tiny treatment compared with saline treatment and with tiny treatment compared with control oligo treatment (Supplemental Figure X). Real-time PCR analysis for 2 direct miR-15 targets, Pdk4 and Sgk1, confirms the microarray analysis and indicate a trending derepression after treatment with tiny 15b (data not shown). The regulation of these genes might be relevant because Pdk4 is a key regulator of mitochondrial function that has been shown to be decreased during hypertrophic remodeling,[22] whereas SGK1 is regulated in response to biomechanical stress and has been shown to inhibit cardiomyocyte apoptosis.[23]

Functional analysis by echocardiography 2 weeks after induction of the ischemic injury indicates that tiny 15b treatment resulted in a significant improvement in ejection fraction, which corresponded with a decrease in both end-systolic and end-diastolic LV volumes (Figure 6F). The improvement in function parallels with a decrease in cardiac fibrosis in response to miR-15 inhibition 2 weeks after injury (Figure 6G). Combined, these data indicate that low doses of tiny 15b during reperfusion can reduce infarct size and improve cardiac function in response to ischemia-reperfusion, which is likely to be at least partially due to a derepression of antiapoptotic genes in response to miR-15 inhibition.

Discussion

Our data show a dynamic time-dependent and regional regulation of miRNAs in porcine cardiac tissue in response to ischemic damage. These changes in porcine cardiac tissue show a large overlap with changes found in a comparable setting in mice and human (reviewed in References 15, 24, and 25).[15,24,25] Most studies to date have shown a decrease in the miR-30 and miR-29 family in response to ischemia, whereas miR-21, miR-199a, miR-210, miR-320, miR-214, miR-92a, and multiple members of the let-7 family consistently show an increase. Although the decrease in the myocyte-specific myo-miRs in the ischemic porcine samples (miR-208a, -208b, and 499) specifically in the infarcted region might be due to a relative decline in myocyte subpopulation, further examination is warranted to determine whether this decreased detection is the result of a regulated process.

Among the regulated miRNAs in the infarcted region is the miR-15 family, which has been implicated in the regulation of cell survival and turnover.[26] Previously, we showed that αMHC-driven, cardiomyocyte-specific overexpression of the miR-15 family member miR-195 resulted in cardiac dilation and premature death around 3 weeks of age. Based on these observations, the proposed function of the miR-15 family and the increased expression in response to hypoxia, we aimed to assess the biological function of the miR-15 family in the setting of ischemic heart disease. In the heart, Bcl2 is involved in myocyte cell loss and contributes to a variety of cardiac pathologies, including heart failure and those related to ischemia/reperfusion injury.[27,28] Previously, miR-15b was shown to increase cardiomyocyte survival in vitro by targeting Arl2, an important regulator of mitochondrial integrity.[6] Although our data confirm that the miR-15 family targets both Bcl2 and Arl2 in cardiomyocytes, the increase in myocyte survival during hypoxia and the protective effect during ischemia-reperfusion on miR-15 inhibition probably is due to the combined effect of many additional gene regulatory changes.

To date, several antisense oligonucleotides have been proven to be efficacious in silencing miRNAs in vivo.[8–12] Whereas cholesterol conjugated antagomirs have been the most widely used experimental approach to inhibit miRNAs, including for cardiac indications, our data indicate LNA-modified oligonucleotide chemistries to be more potent in inhibiting miR function. LNA is a nucleic acid modification

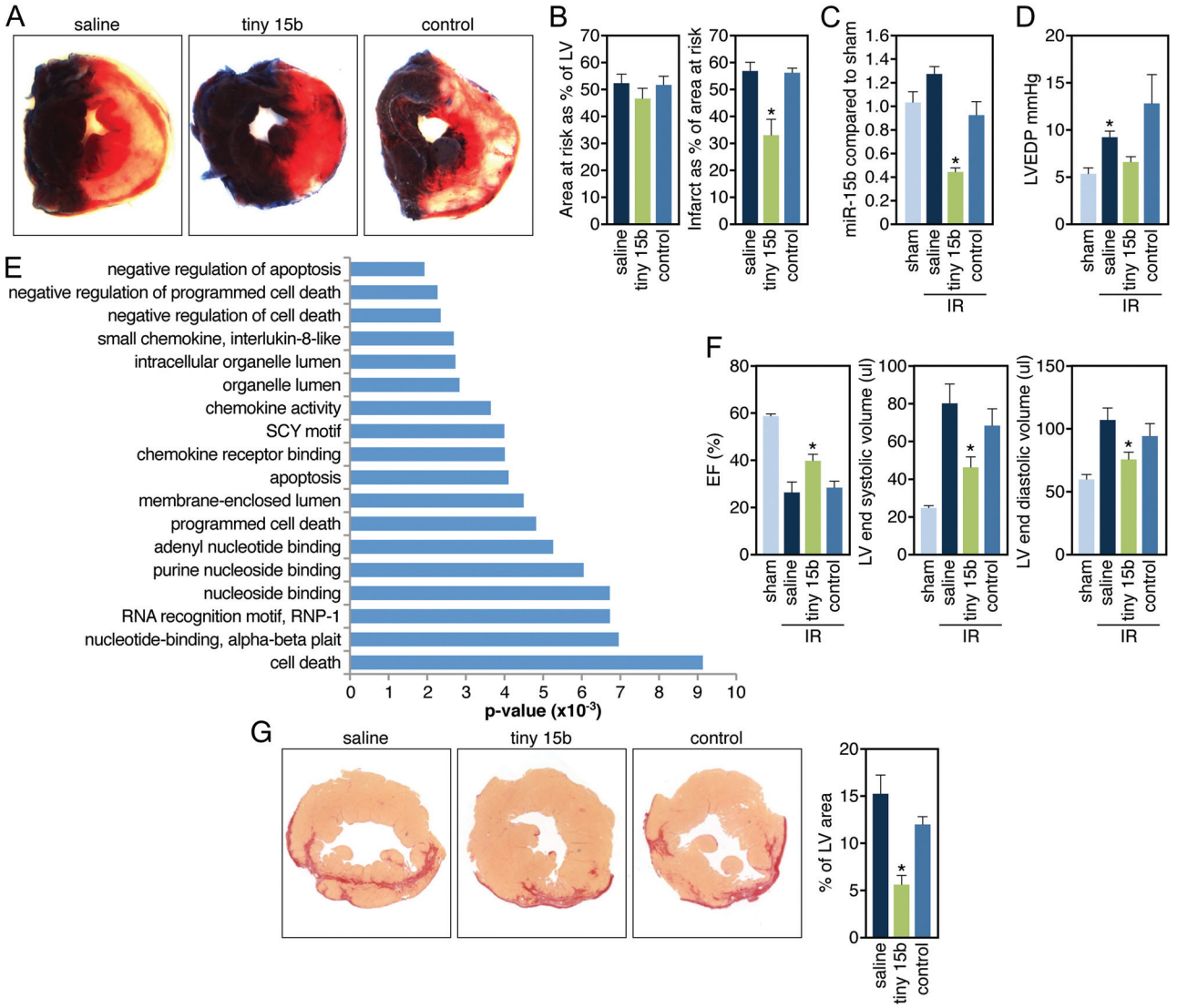

Figure 6. miR-15 inhibition reduces infarct size and improves function in response to ischemia. A, Representative images after TTC staining indicate that although the area at risk (AAR, red and white) is comparable between the different treatment groups, the infarcted area (IA, white) is smaller in the tiny 15b–treated animals (control indicates control oligonucleotide). **B**, Quantification of cross sections of the infarcted hearts indicate that the AAR is ≈50% of the LV for all 3 treatment groups, whereas administration of 0.5 mg/kg of tiny 15b during reperfusion results in a significant reduction in infarct size compared with either saline or control oligo (*$P<0.05$ versus saline and control by ANOVA; control indicates control oligonucleotide). **C**, Real-time PCR analysis on tissue of the ischemic region 24 hours after reperfusion indicates inhibition of miR-15b in response to tiny 15b treatment (*$P<0.05$ versus saline and control oligonucleotide treated by ANOVA). **D**, Left ventricular end-diastolic pressure recordings 24 hours after reperfusion reveals an increase with saline treatment and a reduction with tiny 15b treatment (control indicates control oligonucleotide, *$P<0.05$ versus sham Kruskal-Wallis test). **E**, Ontology analysis of transcripts upregulated ≥1.5-fold in the ischemic region of hearts 24 hours after reperfusion treated with tiny 15b treatment compared with saline, based on microarray profiling. Negative regulators of apoptosis and cell death are significantly overrepresented. **F**, Echocardiography shows a reduction in ejection fraction (EF) and increases in LV volumes 2 weeks after infarct, all of which are significantly improved in response to tiny 15b treatment (*$P<0.05$ versus saline and control by ANOVA for EF and LVESV, versus saline only LVEDV; sham indicates no ischemia/reperfusion; control, control oligo). **G**, Representative images of Picrosirius red–stained cross sections demonstrate a reduction in collagen content of the left ventricle 2 weeks after reperfusion with tiny 15b treatment. Quantification of fibrosis as a percentage of total left ventricular area reveals a statistically significant reduction in the tiny 15b–treated group (*$P<0.05$ versus saline-treated by ANOVA). LV indicates left ventricle.

that introduces a thermodynamically strong duplex formation with oligonucleotides while enhancing specificity toward complementary RNA or DNA, hence allowing for shorter molecules.[8,9] Because microRNA families are frequently more homologous toward their 5′ region, designing a smaller molecule to target the 5′ portion of a miRNA allows for combined targeting of multiple family members in parallel,[29] which was confirmed by our data. The therapeutic applicability of systemically delivered LNA-modified anti-miRs has been reported in nonhuman primates, where inhibition of the liver-expressed miR-122 led to an improvement in hepatitis C virus–induced liver pathology in chronically infected chimpanzees.[12] Recently, we showed LNA-modified oligos to be efficacious in inducing sustained and potent silencing of

cardiac expressed miRNAs.[30,31] Interestingly, the route of administration for these LNA-modified anti-miRs for cardiac targeting is flexible as subcutaneous and intravenous delivery induces a comparable miR-15b inhibition.

Single injections of low amounts of anti-miR induce a potent yet reversible inhibitory effect on their cardiac miRNA target. Because most miRNAs are expressed in many different tissue types, this short duration of action might be beneficial for acute situations, such as protecting myocytes during ischemic injury, to prevent potential side effects caused by miRNA inhibition in extracardiac tissues. More chronic indications probably will warrant multiple doses of anti-miR to sustain inhibition of miRNA, in which case delivery might become more relevant for the ubiquitously expressed miRNAs.

Although we are only just beginning to gain some insights into therapeutic regulation of miRNAs and much more remains to be learned, the fact that they are important regulators during cardiovascular disease together with the feasibility to potently inhibit specific miRNAs, makes them exciting new candidates to target in the setting of heart disease.

Acknowledgments

We gratefully acknowledge our chemistry group for synthesis and purification of the oligonucleotides used in this study. Additionally, we are thankful to Andreas Petri for help with bioinformatic analysis and Jose Cabrera for graphics.

Sources of Funding

E.N.O. was supported by grants from the National Institutes of Health, the Robert A. Welch Foundation, the Donald W. Reynolds Center for Clinical Cardiovascular Research, the Leducq Foundation, and the American Heart Association–Jon Holden DeHaan Foundation.

Disclosures

Except for J.H. and E.N.O., all authors are employees of miRagen Therapeutics, Inc.

References

1. Cannon RO III. Mechanisms, management and future directions for reperfusion injury after acute myocardial infarction. *Nat Clin Pract Cardiovasc Med*. 2005;2:88–94.
2. Wollert KC, Drexler H. Cell therapy for the treatment of coronary heart disease: a critical appraisal. *Nat Rev Cardiol*. 2010;7:204–215.
3. van Rooij E, Sutherland LB, Thatcher JE, DiMaio JM, Naseem RH, Marshall WS, Hill JA, Olson EN. Dysregulation of microRNAs after myocardial infarction reveals a role of mir-29 in cardiac fibrosis. *Proc Natl Acad Sci U S A*. 2008;105:13027–13032.
4. Bartel DP. MicroRNAs: genomics, biogenesis, mechanism, and function. *Cell*. 2004;116:281–297.
5. Small EM, Frost RJ, Olson EN. MicroRNAs add a new dimension to cardiovascular disease. *Circulation*. 2010;121:1022–1032.
6. Nishi H, Ono K, Iwanaga Y, Horie T, Nagao K, Takemura G, Kinoshita M, Kuwabara Y, Mori RT, Hasegawa K, Kita T, Kimura T. MicroRNA-15b modulates cellular ATP levels and degenerates mitochondria through arl2 in neonatal rat cardiac myocytes. *J Biol Chem*. 2010;285:4920–4930.
7. Xia L, Zhang D, Du R, Pan Y, Zhao L, Sun S, Hong L, Liu J, Fan D. Mir-15b and mir-16 modulate multidrug resistance by targeting bcl2 in human gastric cancer cells. *Int J Cancer*. 2008;123:372–379.
8. Elmen J, Lindow M, Schutz S, Lawrence M, Petri A, Obad S, Lindholm M, Hedtjarn M, Hansen HF, Berger U, Gullans S, Kearney P, Sarnow P, Straarup EM, Kauppinen S. LNA-mediated microRNA silencing in non-human primates. *Nature*. 2008;452:896–899.
9. Elmen J, Lindow M, Silahtaroglu A, Bak M, Christensen M, Lind-Thomsen A, Hedtjarn M, Hansen JB, Hansen HF, Straarup EM, McCullagh K, Kearney P, Kauppinen S. Antagonism of microrna-122 in mice by systemically administered LNA-antimir leads to up-regulation of a large set of predicted target mRNAs in the liver. *Nucleic Acids Res*. 2008;36:1153–1162.
10. Krutzfeldt J, Kuwajima S, Braich R, Rajeev KG, Pena J, Tuschl T, Manoharan M, Stoffel M. Specificity, duplex degradation and subcellular localization of antagomirs. *Nucleic Acids Res*. 2007;35:2885–2892.
11. Krutzfeldt J, Rajewsky N, Braich R, Rajeev KG, Tuschl T, Manoharan M, Stoffel M. Silencing of microRNAs in vivo with 'antagomirs.' *Nature*. 2005;438:685–689.
12. Lanford RE, Hildebrandt-Eriksen ES, Petri A, Persson R, Lindow M, Munk ME, Kauppinen S, Orum H. Therapeutic silencing of microRNA-122 in primates with chronic hepatitis C virus infection. *Science*. 2010;327:198–201.
13. Wu Y, Temple J, Zhang R, Dzhura I, Zhang W, Trimble R, Roden DM, Passier R, Olson EN, Colbran RJ, Anderson ME. Calmodulin kinase II and arrhythmias in a mouse model of cardiac hypertrophy. *Circulation*. 2002;106:1288–1293.
14. Gundewar S, Calvert JW, Jha S, Toedt-Pingel I, Ji SY, Nunez D, Ramachandran A, Anaya-Cisneros M, Tian R, Lefer DJ. Activation of amp-activated protein kinase by metformin improves left ventricular function and survival in heart failure. *Circ Res*. 2009;104:403–411.
15. van Rooij E, Fielitz J, Sutherland LB, Thijssen VL, Crijns HJ, Dimaio MJ, Shelton J, De Windt LJ, Hill JA, Olson EN. Myocyte enhancer factor 2 and class II histone deacetylases control a gender-specific pathway of cardioprotection mediated by the estrogen receptor. *Circ Res*. 2010;106:155–165.
16. Gardin JM, Siri FM, Kitsis RN, Edwards JG, Leinwand LA. Echocardiographic assessment of left ventricular mass and systolic function in mice. *Circulation research*. 1995;76:907–914.
17. Cimmino A, Calin GA, Fabbri M, Iorio MV, Ferracin M, Shimizu M, Wojcik SE, Aqeilan RI, Zupo S, Dono M, Rassenti L, Alder H, Volinia S, Liu CG, Kipps TJ, Negrini M, Croce CM. Mir-15 and mir-16 induce apoptosis by targeting bcl2. *Proc Natl Acad Sci U S A*. 2005;102:13944–13949.
18. Koch T, Ørum H. Locked nucleic acids. In: Crooke ST, ed. *Antisense Drug Technology: Principles, Strategies, and Applications*. Boca Raton, FL: CRC Press; 2008.
19. Crouch SP, Kozlowski R, Slater KJ, Fletcher J. The use of ATP bioluminescence as a measure of cell proliferation and cytotoxicity. *J Immunol Methods*. 1993;160:81–88.
20. Corn PG. Hypoxic regulation of mir-210: shrinking targets expand hif-1's influence. *Cancer Biol Ther*. 2008;7:265–267.
21. Levy AP, Levy NS, Loscalzo J, Calderone A, Takahashi N, Yeo KT, Koren G, Colucci WS, Goldberg MA. Regulation of vascular endothelial growth factor in cardiac myocytes. *Circ Res*. 1995;76:758–766.
22. Taegtmeyer H, Razeghi P, Young ME. Mitochondrial proteins in hypertrophy and atrophy: a transcript analysis in rat heart. *Clin Exp Pharmacol Physiol*. 2002;29:346–350.
23. Aoyama T, Matsui T, Novikov M, Park J, Hemmings B, Rosenzweig A. Serum and glucocorticoid-responsive kinase-1 regulates cardiomyocyte survival and hypertrophic response. *Circulation*. 2005;111:1652–1659.
24. Silvestri P, Di Russo C, Rigattieri S, Fedele S, Todaro D, Ferraiuolo G, Altamura G, Loschiavo P. MicroRNAs and ischemic heart disease: towards a better comprehension of pathogenesis, new diagnostic tools and new therapeutic targets. *Recent Pat Cardiovasc Drug Discov*. 2009;4:109–118.
25. Yu S, Li G. MicroRNA expression and function in cardiac ischemic injury. *J Cardiovasc Transl Res*. 2010;3:241–245.
26. Aqeilan RI, Calin GA, Croce CM. Mir-15a and mir-16-1 in cancer: discovery, function and future perspectives. *Cell Death Differ*. 2010;17:215–220.
27. Olivetti G, Abbi R, Quaini F, Kajstura J, Cheng W, Nitahara JA, Quaini E, Di Loreto C, Beltrami CA, Krajewski S, Reed JC, Anversa P. Apoptosis in the failing human heart. *N Engl J Med*. 1997;336:1131–1141.
28. Scarabelli TM, Knight R, Stephanou A, Townsend P, Chen-Scarabelli C, Lawrence K, Gottlieb R, Latchman D, Narula J. Clinical implications of apoptosis in ischemic myocardium. *Curr Probl Cardiol*. 2006;31:181–264.
29. Obad S, dos Santos CO, Petri A, Heidenblad M, Broom O, Ruse C, Fu C, Lindow M, Stenvang J, Straarup EM, Hansen HF, Koch T, Pappin D, Hannon GJ, Kauppinen S. Silencing of microRNA families by seed-targeting tiny LNAs. *Nat Genet*. 2011;43:371–378.

30. Patrick DM, Montgomery RL, Qi X, Obad S, Kauppinen S, Hill JA, van Rooij E, Olson EN. Stress-dependent cardiac remodeling occurs in the absence of microRNA-21 in mice. *J Clin Invest*. 2010;120: 3912–3916.

31. Montgomery RL, Hullinger TG, Semus HM, Dickinson BA, Seto AG, Lynch JM, Stack C, Latimer PA, Olson EN, van Rooij E. Therapeutic inhibition of mir-208a improves cardiac function and survival during heart failure. *Circulation*. 2011;1537–1547.

Novelty and Significance

What Is Known?

- MicroRNAs are important regulators of gene expression.
- MicroRNAs are implicated in the pathogenesis of several diseases.
- MicroRNAs can be therapeutically targeted by oligonucleotide chemistries.

What New Information Does This Article Contribute?

- MicroRNAs are dynamically regulated in response to ischemia-reperfusion injury in the porcine heart.
- Members of the miR-15 family are upregulated in response to ischemic damage and contribute to the disease by regulating cardiac myocyte apoptosis.
- Therapeutic inhibition of the miR-15 family using locked nucleic acid–modified oligonucleotide chemistries induces a protective effect in response to ischemic injury.

Ischemic heart disease is a major cause of congestive heart failure, a leading cause of death worldwide. In an attempt to further define the regulatory mechanisms that contribute to heart failure, we examined changes in microRNA (miRNA) levels in response to ischemia in pig hearts. Our data indicate that multiple members of the miR-15 family are upregulated in response to ischemia. Modified oligonucleotides directed against this miRNA family effectively suppressed expression of miR-15 family members in vitro and rendered cardiac myocytes resistant to hypoxia-induced cell death. Correspondingly, systemic delivery of miR-15 anti-miRs dose-dependently repressed miR-15 in cardiac tissue of both mice and pigs. Therapeutic targeting of miR-15 in mice reduced infarct size and cardiac remodeling and enhanced cardiac function after ischemic cardiac injury. These studies represent an important step toward optimization of oligonucleotide-based therapies for modulation of cardiac miRNAs and validate miR-15 as a therapeutic target for the manipulation of cardiac remodeling and function in the settings of ischemic heart disease.

Supplemental material

Inhibition of miR-15 protects against cardiac ischemic injury

Thomas G. Hullinger[1], Rusty L. Montgomery[1], Anita G. Seto[1], Brent A. Dickinson[1], Joshua M. Lynch[1], Christina M. Dalby[1], Kathryn Robinson[1], Christianna Stack[1], Paul A. Latimer[1], Joshua M. Hare[2], Eric N. Olson[3] and Eva van Rooij [1]*

Porcine IR surgery All animal studies were approved by the Institutional Animal Care and Use Committee and comply with the Guide for the Care and Use of Laboratory Animals (National Institutes of Health Publication no. 80-23, revised 1985). Female Yorkshire pigs underwent 60-minute balloon occlusion of the left anterior descending coronary artery (LAD) followed by reperfusion. Animals were sacrificed either 2 or 8 weeks post-MI. At autopsy, samples of infarcted myocardium, border zone, and remote zone were obtained. Female Yourshire pigs (age = 3 months, weight 25-30 kg) were subjected to closed-chest infarction, in which myocardial infarction is induced by inflation of a coronary angioplasty balloon in the left anterior descending artery. Coronary angiography was performed in Female Yourshire pigs (n=4) via an 8 F intravascular sheath in the right carotid artery, using a right Judkins catheter under fluoroscopic guidance. Myocardial infarction was induced by inflating a coronary angioplasty balloon (2.5 × 20 mm) in the proximal left anterior descending coronary artery for 60 min, followed by reperfusion. All animals were pretreated with lidocaine, and adequately heparinized during the surgical procedure. After reperfusion, the catheter sheath in the carotid artery was removed, and the carotid artery was permanently closed.

Murine IR surgery 7-8 wk old C57Bl6 male mice were anesthetized with intraperitoneal injections of ketamine (50 mg/kg) and sodium pentobarbital (60 mg/kg), intubated and placed on a rodent ventilator. An ip injection of sodium heparin (200 Units/kg) was administered and body temperature was maintained at 37°C with a heating pad and monitored during the experimental procedure via a rectal probe. The heart was accessed via the third intercostal space on the left side. A decending branch of the left coronary artery was identified and ligated against a short piece of PE10 tubing just distal to the left atrial appendage with 7-0 silk suture. Ligation was confirmed by distal cyanosis. After 75 minutes of ischemia, the PE10 tubing was removed and the suture cut to allow for reperfusion. Reperfusion was confirmed by reactive hyperemia and the surgical site was closed. Upon return of spontaneous breathing, the mice were placed in a warm recovery cage and returned to normal housing conditions when fully ambulatory.

Infarct size determination At 24 hours of reperfusion, the mice were anesthetized, intubated, and connected to a rodent ventilator. A catheter (PE-10 tubing) was placed in the common carotid artery to allow for Evans Blue dye injection. A median sternotomy was performed and the left main coronary artery was re-ligated in the same location as before. Evans Blue dye (1.2 mL of a 2.0% solution, Sigma) was injected into the carotid artery catheter into the heart to delineate the ischemic zone from the nonischemic zone. The heart was rapidly excised and serially corss sectioned in five, 1 mm thick sections that were then incubated in 1.0% 2,3,5-triphenyltetrazolium chloride (Sigma) for 5 minutes at 37°C to demarcate the viable and nonviable myocardium within the area at risk. Each of the 5, 1 mm thick myocardial slices were

weighed and the areas of infarction, risk, and nonischemic left ventricle were assessed by a blinded observer using computer-assisted planimetry (NIH Image 1.57).

Echocardiography Cardiac function and heart dimensions were evaluated by two-dimensional echocardiography in mice sedated with 5% isoflurane using a Visual Sonics Vevo 770 Ultrasound (Visual Sonics, Canada) and a 30-MHz linear array transducer. M-mode tracings were used to measure anterior and posterior wall thicknesses at end diastole and end systole. Left ventricular (LV) internal diameter (LVID) was measured as the largest anteroposterior diameter in either diastole (LVIDd) or systole (LVIDs). The data were analyzed by a single observer blinded to treatment. LV fractional shortening (FS) was calculated according to the following formula: FS (%) = [(LVIDd - LVIDs)/LVIDd] x 100.

Microarray for miRNAs Microarray assay was performed using a service provider (LC Sciences, Houston).The assay started from 10 µg total RNA sample, which was size fractionated using a YM-100 Microcon centrifugal filter (from Millipore) and the small RNAs (< 300 nt) isolated were 3'-extended with a poly(A) tail using poly(A) polymerase. An oligonucleotide tag was then ligated to the poly(A) tail for later fluorescent dye staining; two different tags were used for the two RNA samples in dual-sample experiments. Hybridization was performed overnight on a µParaflo microfluidic chip containing detection probes consisting of a chemically modified nucleotide coding segment complementary to target microRNA (from miRBase, http://microrna.sanger.ac.uk/sequences/) or other RNA (control or customer defined sequences). The hybridization melting temperatures were balanced by chemical modifications of the detection probes. After RNA hybridization, tag-conjugating Cy5 dyes were circulated through the microfluidic chip for dye staining. Fluorescence images were collected using a laser scanner (GenePix 4000B, Molecular Device) and digitized using Array-Pro image analysis software (Media Cybernetics). The ratio of the detected signals (log2 transformed, balanced) and p-values of the t-test were calculated, and differentially detected signals were those with less than 0.01 p-values.

Cell Culture and luciferase assays HeLa cells were purchased from ATCC and cultured in Minimum Essential Media with Earle's Balanced Salt Solution (Hyclone) supplemented with 2mM L-Glutamine, 1mM Sodium Pyruvate, 1nM Non-essential Amino Acids, and 10% FBS (PAA). Rat neonatal myocytes were obtained from Neonatal Sprague Dawley rats 24-48hrs after birth. Neonates remained with their mothers until the start of the protocol. Pups were, counted,weighed, cleaned with ethanol and decapitated. The heart was removed and placed in a harvesting solution on ice. The left and right ventricles were minced in a laminar flow hood and tissue was placed in a spinner flask containing digestion solution (1.5-2mg/ml trypsin). Tissue was washed and digested at 35°C in twelve 5-10min steps, collecting the myocyte containing supernatant after each step. The supernatant was spun in a centrifuge to isolate cells which were resuspended in Minimal Essentials Media (MEM). Cells were pooled, run through a 100µm cell strainer, and re-spun . Myocytes were purified by plating in culture dishes at 1% CO_2 for 45min allowing non-myocyte material to adhere to plates. The cardiac myocytes in solution were then counted, diluted, and plated for experiments and assays.
HeLa cells were plated in serum-containing media without antibiotics in 96-well plates (1 x 10^4 cells/well) 24 hours prior to transfection. Cell were transfected with 8.3 nanomol/L (nM) to 309 picomol/l (pM) inhibitor and 25 ng/well of the reporter plasmid using 0.3µL/well Lipofectamine 2000 (Life Technologies, Cat # 11668-019). Reporter plasmids were prepared as previously described (Vermeulen 2007). Cells were grown at 37°C and harvested 24 hours post transfection for luciferase assays. Firefly and *Renilla* luciferase activities were measured using the Dual-Glo Luciferase Assay System (Promega, Cat #E2940) according to manufacturer's

instructions except for the following modification. The growth media was aspirated from the cells and 50µL of 1X PBS was added to each well prior to adding 50µL of firefly luciferase substrate and 50µL *Renilla* luciferase substrate.
Neonatal rat cardiomyocytes were isolated as previously described and plated on Primaria coated plates at 80,000 cells per well (24 well) or 600,000 cells per well (6 well). During the isolation, cells are plated in Minimum Essential Media with Hank's Balanced Salt Solution (Invitrogen) supplemented with 5% Calf Serum (CO serum company) 50,000U/mL PCN, 2mg/mL B12, and 1% BrdU (to prevent fibroblast proliferation). 24hr after isolation, cells are serum starved in Minimum Essential Media with Hank's Balanced Salt Solution (Invitrogen) supplemented with 1mg/mL insulin, 1mg/ml transferring, 100mg/mL BSA, and 1%BrdU. 24hr later, cells are transfected in this same media, but with the addition of 0.1% calf serum. Cells are transfected with1ug/well (24 well) or 3ug/well (6 well) Dharmafect 2 (Thermofisher Scientific) as per the manufacturers' instructions.

Northern blot analysis Total RNA was isolated from porcine or mouse cardiac tissue samples by using Trizol reagent (Gibco/BRL). Northern blots to detect microRNAs were performed and a U6 probe served as a loading control (IDT). Northern blot analysis for the experiments in which LNA-modified antimiR chemistries were used were electrophoresed on non-denaturing gels to show the heteroduplex formation between the LNA and mature miRNAs. Briefly, 12 ug of total heart RNA was loaded unheated on a native 20% acrylamide gel, run for 1.5 hours at 150V, and transferred to a Zeta-probe blotting membrane (Bio-rad) for 2 hours at 90V. Membranes were probed with a ^{32}P-labelled LNA-modified oligonucleotide for the indicated miRNAs (Exiqon) and hybridized overnight at 37°C using RapidHyb buffer (GE Healthcare). Blots were visualized using a Storm 860 scanner (Molecular Dynamics).

Biodistribution assay To determine the presence of the antimiRs either in plasma or tissues we used a Hybridization Assay Method to detect the L/D 15b and a competition assay for the tiny 15b. Probes for the hybridization assay were synthesized using 2'Ome modified nucleotides and are: UCAUGGU-bTEG (capture probe) and 6FAM-AGCAGCACA (detect probe). Detection was accomplished using anti-fluorescence-POD, Fab fragments (Roche) and TMB Peroxidase Substrate (KPL). Standard curves were generated using non-linear logistic regression analysis with 4 parameters (4-PL). The working concentration range of the assay was 0.021-5.37 ng/ml. Tissue samples were prepared at 100mg/ml by homogenizing in 3M GITC buffer (3 M guanidine isothiocyanate, 0.5 M NaCl, 0.1 M Tris pH 7.5, 10 mM EDTA) for 2x 30 seconds using an MP FastPre-24 at a speed setting of 6.0. Plasma samples and tissue homogenates were diluted a minimum of 50-fold in 1 M GITC Buffer (1 M guanidine isothiocyanate, 0.5 M NaCl, 0.1 M Tris pH 7.5, 10 mM EDTA) for testing. The competition hybridization assay was used for the quantification of tiny 15b in plasma and tissue samples. A biotinylated, 2'Ome modified capture oligo, complementary to the tiny 15b sequence (bTEG-AGCAGCAC), was bound to a strepavidin coated 96-well plate. An equal mol amount of a 6FAM-Tiny15b competition probe was added to all samples and standard curve dilutions prior to adding samples and dilutions to the capture plate. Detection was accomplished using anti-fluorescence-POD, Fab fragments (Roche) and TMB Peroxidase Substrate (KPL). A standard curve was generated using non-linear logistic regression analysis with 4 parameters (4-PL) such that signal was inversely proportional to tiiny 15b concentration. The working concentration range of the assay was 0.272-139 ng/ml. Tissue samples were prepared at 100mg/ml by homogenizing in 3M GITC buffer (3 M guanidine isothiocyanate, 0.5 M NaCl, 0.1 M Tris pH 7.5, 10 mM EDTA) for 2x 30 seconds using an MP FastPre-24 at a speed setting of 6.0. Plasma samples and tissue homogenates were diluted a minimum of 50-fold in 1 M GITC Buffer (1 M guanidine isothiocyanate, 0.5 M NaCl, 0.1 M Tris pH 7.5, 10 mM EDTA) for testing.

Online Table I: Microarray analysis on porcine cardiac samples both 2 and 8 weeks after IR injury in the infarct region.

	infarct region			Log2	
miRNA	**control**	**2 wks post-IR**	**8 wks post-IR**	**2 wks vs control**	**8 wks vs control**
let-7b	12,892	22,674	17,654	0.81	
let-7e	9,678	11,547	5,335		-0.86
let-7g	7,670	7,344	3,036		-1.34
let-7i	5,763	13,083	5,470	1.18	
miR-1	26,527	4,539	14,236	-2.55	-0.90
miR-100	7,760	11,996	5,906	0.63	-0.39
miR-101	483	108	24	-2.16	-4.05
miR-101a	645	117	58	-2.46	-3.48
miR-106a	1,007	808	349		-1.53
miR-106b	546	439	298		-0.88
miR-125a-5p	3,798	8,951	6,205	1.24	0.71
miR-126	19,404	15,418	8,486	-0.33	-1.19
miR-127-3p	109	402	352	1.88	1.69
miR-1275	35	334	167	3.24	
miR-128	1,281	415	1,025	-1.62	
miR-1280	159	94	403	-0.75	
miR-1281	66	65	565		3.09
miR-1308	65	397	1,065	2.62	4.04
miR-130a	704	481	356	-0.55	-0.98
miR-133a	17,945	4,584	30,657	-1.97	
miR-133b	17,837	4,197	29,645	-2.09	0.73
miR-139-5p	293	160	260	-0.88	
miR-140*	329	1,050	1,528	1.67	
miR-140-3p	303	807	1,246	1.42	2.04
miR-143	6,737	8,424	4,204		-0.68
miR-145	7,986	11,727	14,667	0.55	0.88
miR-1468	255	50	147	-2.34	
miR-1469	64	330	604		3.25
miR-146b	18	228	17	3.68	
miR-148a	376	1,906	75	2.34	-2.32
miR-150	420	1,007	473	1.26	
miR-151-5p	2,146	3,328	2,601	0.63	
miR-152	1,037	2,259	287	1.12	-1.85
miR-155	5	330	6	6.15	
miR-15a	1,305	1,159	128		-3.35
miR-15b	1,137	2,837	1,335	1.32	
miR-16	8,350	9,174	4,841		-0.79
miR-17	1,119	839	455		-1.30
miR-17-5p	1,234	935	443	-0.40	-1.48
miR-18	35	28	13		
miR-181a	1,681	2,317	3,318	0.46	1.15
miR-181d	169	127	78		-1.14
miR-1826	3,344	5,923	6,381	0.83	0.93
miR-185	248	447	285	0.85	
miR-186	223	118	104	-0.92	
miR-191	4,198	6,476	5,068	0.63	
miR-193a-5p	104	315	327	1.60	1.66
miR-195	2,314	3,355	776	0.54	-1.58
miR-1977	471	21	779	-4.50	0.73
miR-1978	1,251	249	6,041	-2.33	2.27

	infarct region			Log2	
miRNA	control	2 wks post-IR	8 wks post-IR	2 wks vs control	8 wks vs control
miR-1979	972	4,486	6,552	2.21	2.75
miR-199a-3p	5,660	18,144	4,300	1.68	
miR-199b-5p	486	950	132	0.97	-1.88
miR-19b	820	284	118	-1.53	
miR-208b	5,223	297	1,069	-4.14	
miR-20a	1,255	896	351		-1.84
miR-21	1,492	15,775	737	3.40	-1.02
miR-214	1,757	14,367	4,668	3.03	1.41
miR-22	5,647	1,867	5,636	-1.60	
miR-22*	352	72	96	-2.28	
miR-221	118	421	181	1.73	
miR-222	80	282	322	1.83	2.02
miR-23a	19,139	27,346	25,171	0.51	0.40
miR-25	1,166	2,371	1,261	1.02	
miR-26b	4,892	3,210	1,048		-2.22
miR-27a	11,802	9,563	8,392		-0.49
miR-29a	3,737	2,217	3,845	-0.88	
miR-29b	107	13	25	-3.00	-2.04
miR-29c	4,785	423	1,653	-3.50	-1.53
miR-30a	9,375	2,750	5,275	-1.77	
miR-30b	21,719	11,873	16,754	-0.87	
miR-30c	12,516	6,677	12,549	-0.91	
miR-30d	7,662	2,895	5,602	-1.40	
miR-30e	5,853	541	1,396	-3.44	-2.07
miR-30e*	771	77	216	-3.32	-1.83
miR-320a	1,291	3,881	2,423	1.59	0.91
miR-320b	1,149	3,569	1,907	1.64	0.73
miR-320c	1,265	3,940	2,322	1.64	0.88
miR-320d	431	1,308	684	1.60	0.67
miR-329	900	669	4,715	-0.43	2.39
miR-374b	160	205	29		-2.52
miR-378	4,787	435	4,625	-3.46	
miR-422a	1,067	18	251	-5.85	-2.09
miR-423-5p	317	702	1,029	1.15	1.70
miR-424	571	855	60	0.58	-3.45
miR-451	10,194	14,589	3,198	0.52	-1.67
miR-455-3p	269	972	606	1.85	1.17
miR-484	55	37	196		1.82
miR-486-5p	989	153	3,023	-2.69	1.61
miR-498	37	31	265		2.86
miR-499-5p	16,931	3,014	7,492	-2.49	-1.18
miR-548m	95	52	558		2.56
miR-574-3p	56	468	276	3.07	2.30
miR-582-5p	348	6	22	-4.66	-4.23
miR-638	605	2,615	6,132	2.11	3.34
miR-652	300	37	380	-3.04	
miR-663	24	133	232	2.44	3.25
miR-92a	1,722	2,843	2,848	0.72	0.73
miR-92b	390	727	689	0.90	0.82
miR-940	37	45	187		2.35
miR-98	546	494	53		-3.36
miR-99a	8,657	13,749	6,737	0.67	

Online Table II: Microarray analysis on porcine cardiac samples both 2 and 8 weeks after IR injury in the borderzone region.

	borderzone region			Log2	
miRNA	control	2 wks post-IR	8 wks post-IR	2 wks vs control	8 wks vs control
let-7d	15,798	19,830	6,344		-1.32
let-7e	8,793	8,492	2,139		-2.04
let-7f	14,799	17,013	4,595	0.20	-1.69
let-7g	6,671	5,843	1,441		-2.21
let-7i	5,861	12,326	4,189	1.07	-0.92
miR-1	25,328	12,019	5,650	-1.08	-2.16
miR-107	1,987	1,633	2,518	-0.28	
miR-1224-5p	166	98	412		1.31
miR-126	18,606	12,244	7,362	-0.60	-1.34
miR-127-3p	159	383	251	1.27	
miR-1275	61	136	296		2.27
miR-1277	44	66	405		3.19
miR-128	1,425	724	946	-0.98	-0.59
miR-1280	153	129	663		2.12
miR-1308	57	1,142	265	4.33	
miR-130a	593	450	167		-1.51
miR-133a	19,841	10,975	52,839	-0.85	1.41
miR-133b	19,213	10,098	50,154	-0.93	1.38
miR-139-5p	390	79	140	-2.31	
miR-140*	508	1,041	1,592	1.03	1.65
miR-140-3p	418	1,028	1,143	1.30	1.45
miR-143	6,731	7,767	5,033		-0.42
miR-145	9,504	11,949	15,356		0.69
miR-1468	233	45	17		-3.77
miR-1469	97	152	2,762		4.83
miR-146b	12	182	9	3.88	
miR-148a	320	1,131	58	1.82	-2.51
miR-149*	23	40	397		4.09
miR-150	629	823	380		-0.72
miR-151-3p	378	460	629		0.73
miR-152	873	1,273	89	0.54	-3.29
miR-15a	827	569	73		-3.51
miR-15b	1,328	1,935	220	0.54	-2.60
miR-16	8,005	9,678	3,442		-1.22
miR-181a	1,922	2,500	3,629		0.73
miR-1826	6,368	5,979	13,222		1.05
miR-193a-5p	207	330	586		1.50
miR-195	2,046	1,911	374		-2.45
miR-1977	612	105	655	-2.54	
miR-1978	2,378	520	10,725	-2.19	2.17
miR-1979	1,589	2,659	10,273		2.69
miR-199a-3p	5,148	17,106	2,139	1.73	-1.27
miR-199b-5p	341	704	35	1.05	
miR-19b	529	318	83		-2.67
miR-208b	3,295	1,239	961	-1.41	-1.78
miR-20a	1,036	819	323	-0.34	-1.68
miR-20b	145	54	21		
miR-21	635	12,201	38	4.26	-4.06
miR-214	2,760	10,443	5,319	1.92	0.95
miR-22*	258	54	54	-2.27	

	borderzone region			Log2	
miRNA	control	2 wks post-IR	8 wks post-IR	2 wks vs control	8 wks vs control
miR-221	121	646	75	2.41	
miR-222	104	719	304	2.78	1.54
miR-23a	17,934	29,494	19,844	0.72	
miR-23b	23,499	34,461	26,773	0.55	
miR-26b	3,066	1,810	153	-0.76	-4.33
miR-27a	10,949	8,936	5,309		-1.04
miR-27b	16,115	14,447	10,321		-0.64
miR-28	509	418	179		-1.51
miR-29c	3,588	647	1,529	-2.47	-1.23
miR-30a	8,242	3,376	5,025	-1.29	
miR-30e	4,155	1,232	1,942	-1.75	-1.10
miR-30e*	569	89	26	-2.67	-4.45
miR-320a	1,549	2,482	3,741	0.68	1.27
miR-320b	1,389	1,840	2,348		0.76
miR-320c	1,568	2,393	3,133	0.61	1.00
miR-331-3p	160	71	968		2.60
miR-34a	173	448	387	1.37	1.16
miR-352	597	374	90	-0.68	-2.73
miR-378	5,168	1,146	6,825	-2.17	
miR-422a	1,089	20	35	-5.78	-4.96
miR-423-5p	551	450	3,583		2.70
miR-424	300	363	22		-3.79
miR-451	11,144	10,724	4,371		-1.35
miR-455-3p	358	999	483	1.48	
miR-484	70	64	477		2.78
miR-486-5p	1,352	313	6,836	-2.11	2.34
miR-498	67	66	466		2.80
miR-499-5p	15,552	9,018	5,899	-0.79	-1.40
miR-548m	149	239	1,049		3.06
miR-574-5p	21	111	70	2.43	
miR-582-5p	242	30	21	-3.01	-2.78
miR-638	1,001	1,075	16,545		4.05
miR-652	389	86	316	-2.19	
miR-663	51	62	1,070		4.39
miR-720	57	127	659		3.52
miR-92b	571	468	381		-0.58

OnlineTable III: Upregulated genes in response to tiny 15b inhibition compared to saline treatment, as measured by microarray profiling.

GENE SYMBOL	FOLD CHANGE		
Myl4	12.46	Ptp4a3	2.425
Adh1	7.80	Taf15	2.413
E030010A14Rik	6.51	LOC100046744	2.402
Hspa1a	5.81	LOC100047674	2.398
Rhoj	5.76	Pam	2.387
Kcne1	5.17	Mtmr3	2.304
Ptx3	4.58	Kcne4	2.291
Ptx3	4.50	Cnot6l	2.287
Jph2	4.29	Kif1b	2.276
Chrm2	4.03	Gadd45a	2.219
Abhd2	3.96	Glul	2.217
Mobkl2c	3.67	4732471D19Rik	2.190
Klf10	3.57	Ccng2	2.169
Pdk4	3.54	Slc22a9	2.164
BC055107	3.38	2010107G12Rik	2.149
Arntl	3.20	Cxcl14	2.149
Il6	3.20	LOC381066	2.143
Fosb	3.09	Hdc	2.130
Phka2	3.02	Pxmp4	2.129
Rnf125	3.00	Ddx6	2.125
Slc10a6	2.92	8430408G22Rik	2.116
Med1	2.89	Cxcl9	2.115
Smad5	2.87	Car14	2.102
Kremen2	2.85	Pwp1	2.086
Cxcl1	2.81	Prpf40a	2.086
Ccl11	2.79	Fus	2.063
Bmp4	2.77	6230427J02Rik	2.048
Cyp1b1	2.73	Cbx7	2.046
Camk2d	2.73	Cdc37l1	2.044
Tm4sf20	2.71	Rell1	2.037
Sphk1	2.71	Cfl1	2.036
Cd33	2.63	Aqp1	2.035
Gadd45b	2.61	Mt2	2.017
Gtl3	2.60	Nampt	2.009
Trp53inp1	2.59	Rnf125	2.007
LOC100046802	2.57	Cry2	2.003
Slc10a6	2.47	Sfrs5	2.002
Cdkn1a	2.44	Cdkn1a	1.986
Mical1	2.44	Map3k6	1.983
Retnlg	2.43	Pgf	1.974
1190002H23Rik	2.43	Chac1	1.967

Pak6	1.945	Aqp1	1.809
Tgfbr1	1.940	Id2	1.809
Taf5l	1.936	Cycs	1.807
Plscr2	1.933	Cblb	1.807
C230071H18Rik	1.928	Pik3r1	1.804
Sema6b	1.928	Polr3k	1.803
D17Wsu92e	1.922	Dcbld1	1.802
Camk2d	1.921	Sesn1	1.801
Prei4	1.909	Tnfsf13b	1.801
Auts2	1.909	Egr1	1.799
Plekhf1	1.908	EG665378	1.796
Ube2j1	1.904	Pik3r1	1.795
Pet112l	1.904	Sdcbp2	1.794
Ywhae	1.903	Pgm5	1.791
Cldn5	1.903	Akap12	1.790
Cyfip2	1.899	Phf20l1	1.790
Zfp35	1.888	H2-Q8	1.787
Trp53i11	1.883	Socs3	1.786
Slc41a3	1.881	Fgf1	1.784
Rora	1.879	Arhgap26	1.783
Trim16	1.876	LOC100047200	1.780
Pcmt1	1.873	Myd116	1.777
Scd1	1.873	Metrn	1.775
Txnip	1.869	Tbx3	1.775
Rerg	1.867	Pim3	1.767
LOC100047052	1.861	Lass4	1.764
Traf6	1.859	Lrrc10	1.756
Hsp90aa1	1.856	Lepre1	1.753
Ap2b1	1.853	Acsl4	1.752
Klf9	1.849	Josd3	1.748
Arl6ip2	1.843	Ddit4	1.747
Tmem2	1.841	Rp23-297j14.5	1.746
Cdkn1a	1.841	Dhdds	1.745
Sox17	1.839	Runx1	1.744
Irs2	1.839	Arrdc4	1.743
3632451O06Rik	1.832	Slc19a2	1.743
Magi1	1.828	Rnf25	1.737
Samd8	1.815	Eif4g2	1.737
Itpkc	1.811	4932702K14Rik	1.737
Stc2	1.810	Plscr1	1.734
Zfand6	1.810	Slc20a1	1.724

Hcfc2	1.724	2310047M10Rik	1.647
Ndufb9	1.720	Bat2	1.644
Timp4	1.710	Znrf1	1.644
Timp3	1.709	Ddt	1.644
Lphn1	1.705	Grap	1.641
E130309D02Rik	1.705	Plekhf2	1.639
Pparg	1.705	Peli1	1.639
Gpr176	1.704	Asnsd1	1.634
Wdr13	1.703	Actb	1.631
Gadd45a	1.698	Cxcl2	1.625
Asb11	1.691	Mccc1	1.625
Pxdn	1.690	Rbm18	1.624
Actb	1.686	Ptp4a2	1.623
Slc12a4	1.685	Wdr32	1.620
Msi2h	1.682	Acsl3	1.614
LOC100047261	1.676	Gata2	1.609
Foxn3	1.676	Sfrs6	1.608
Prkrip1	1.673	Myh6	1.605
Fkbp5	1.672	Arl4a	1.603
Wnk1	1.668	Fem1c	1.600
Setd5	1.668	Egfr	1.600
U2af1l4	1.668	Angptl4	1.599
Edg2	1.667	Mllt3	1.597
Serf1	1.666	Selp	1.597
Dyrk1a	1.665	Cdc42ep4	1.596
Hhatl	1.664	Trex1	1.595
Il20rb	1.663	Eif4e	1.592
Ndufb4	1.662	Fut4	1.590
BC027231	1.661	Twistnb	1.589
Trem1	1.660	Prpf38b	1.588
Nfkbia	1.654	Mical1	1.588
Zrsr2	1.654	Cnot4	1.587
Dock4	1.653	Alg6	1.587
Bcl2l1	1.653	Tsc22d3	1.586
Sbno2	1.651	Sox17	1.585
Tob2	1.650	Plekha5	1.580
Ptrh2	1.649	Atp1a2	1.575
LOC100047856	1.649	Sele	1.574
Hsf2	1.649	Dpp8	1.572
Arrdc2	1.647	Jmjd2b	1.571
Etv6	1.647	Ch25h	1.570

1810015C04Rik	1.570
Brd8	1.567
Srgn	1.566
Siah1a	1.566
Mtmr1	1.564
Farsa	1.563
Pgrmc1	1.562
Dennd3	1.562
H2-Q7	1.562
Tatdn2	1.558
Map3k8	1.558
Sox5	1.558
Psmb8	1.558
LOC547343	1.555
Kcnq2	1.554
Chmp5	1.554
Enc1	1.553
Phca	1.553
LOC100048858	1.552
Lrtm1	1.552
Kpna3	1.551
Mlf1	1.550
Ddx6	1.549
Scube2	1.549
1700025K23Rik	1.548
Zbtb2	1.547
2610528E23Rik	1.547
Ctdp1	1.546
Fcgr2b	1.546
Osbpl6	1.544
Gtf3c4	1.544
Aqp1	1.544
Hspa5	1.543
Rtn2	1.543
AA467197	1.541
Ltbp1	1.540
E4f1	1.540
Hadhsc	1.540
Atm	1.538
Pla1a	1.538
Ubac1	1.536
Sparcl1	1.536
Zc3h7a	1.536
Dld	1.536
Ddx3x	1.534
Dnaja2	1.533
Sgk1	1.533
Clec1a	1.532
Wbscr16	1.532
Trim2	1.531
Atp5a1	1.531
Armetl1	1.529
Suv420h1	1.528
Ypel5	1.525
Habp4	1.524
Spsb1	1.524
Ttc3	1.523
Gbp3	1.522
Ddx58	1.518
Bckdhb	1.518
Tbp	1.518
Mat2a	1.517
P2ry14	1.517
A330080J22Rik	1.517
Sdhd	1.514
Fas	1.513
Josd3	1.511
Mpdz	1.511
Tcea3	1.510
Pcdh17	1.510
Plcb4	1.510
Junb	1.509
Zc3h12a	1.505
Prodh	1.503
Jmjd3	1.501
Ebf1	1.501

Online Table IV: Expanded list of gene ontology terms (p-value < 0.05).

Term	Functional classification	P-value
GO:0043066	negative regulation of apoptosis	0.001928
GO:0043069	negative regulation of programmed cell death	0.002267
GO:0060548	negative regulation of cell death	0.002345
IPR001811	Small chemokine, interleukin-8-like	0.002685
GO:0070013	intracellular organelle lumen	0.002728
GO:0043233	organelle lumen	0.002834
GO:0008009	chemokine activity	0.003644
SM00199	SCY	0.003997
GO:0042379	chemokine receptor binding	0.004008
GO:0006915	apoptosis	0.004104
GO:0031974	membrane-enclosed lumen	0.004496
GO:0012501	programmed cell death	0.004819
GO:0030554	adenyl nucleotide binding	0.005259
GO:0001883	purine nucleoside binding	0.006050
GO:0001882	nucleoside binding	0.006725
IPR000504	RNA recognition motif, RNP-1	0.006727
IPR012677	Nucleotide-binding, alpha-beta plait	0.006954
GO:0008219	cell death	0.009132
GO:0016265	death	0.011300
SM00360	RRM	0.013122
GO:0006606	protein import into nucleus	0.013128
GO:0051170	nuclear import	0.014788
GO:0034504	protein localization in nucleus	0.017517
GO:0030335	positive regulation of cell migration	0.022230
GO:0051272	positive regulation of cell motion	0.029090
GO:0051603	proteolysis involved in cellular protein catabolic process	0.029388
GO:0044257	cellular protein catabolic process	0.030475
domain	CUB	0.034599
GO:0040017	positive regulation of locomotion	0.034887
GO:0046872	metal ion binding	0.039987
GO:0030163	protein catabolic process	0.040276
active site	Phosphocysteine intermediate	0.041814
GO:0050670	regulation of lymphocyte proliferation	0.041898
GO:0032944	regulation of mononuclear cell proliferation	0.041898
GO:0017038	protein import	0.045202
GO:0070663	regulation of leukocyte proliferation	0.045202
GO:0043169	cation binding	0.048263
IPR016130	Protein-tyrosine phosphatase, active site	0.049231

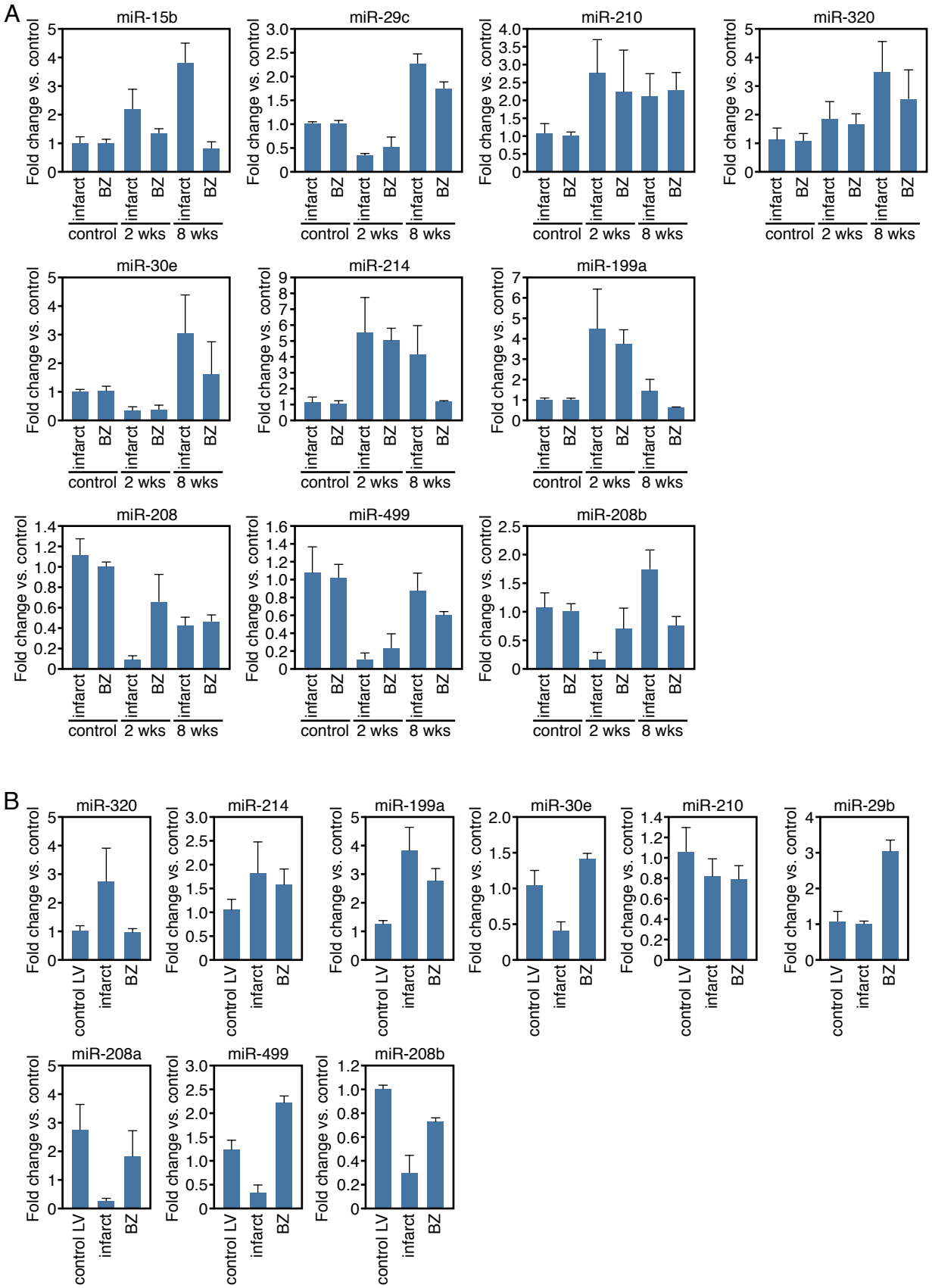

Online figure I. Dynamic regulation of miRNAs in cardiac porcine tissue after ischemic injury.

A. Realtime PCR analysis on both infarct and borderzone material 2 and 8 weeks after ischemic injury in pigs confirming the regulation of microRNAs as indicated by microarray analysis (BZ=border zone).

B. Realtime PCR analysis on both infarct and borderzone material after 90 minutes of ischemia and 24 hrs of reperfusion showing the dynamic regulation of miRNAs in response to shortterm ischemic damage.

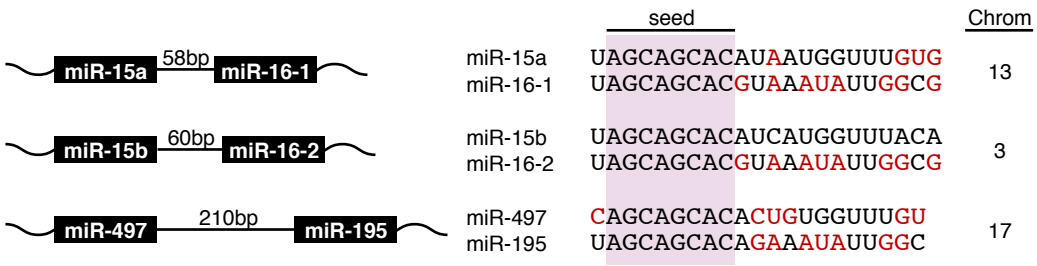

Online figure II. miR-15 family.
The miR-15 family consists of 6 members (miR-15a, -15b, -16, -195 and miR-497) that are expressed as 3 bicistronic clusters. While they are conserved in their seed sequence, the members differ significantly in their 3′ sequences (as indicated in red).

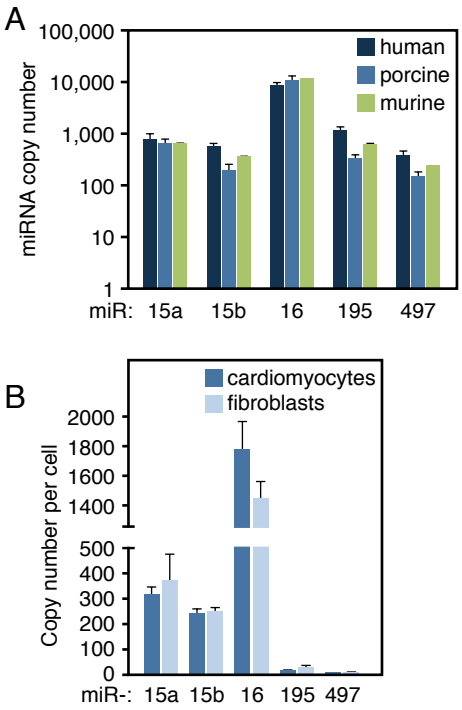

Online figure III. Relative abundance of the different miR-15 family members across species.

A. Based on the assumption that there are roughly 20 million cells in a mouse heart (~10pg RNA/cell) quantitative realtime PCR analysis using a pool of synthetic microRNAs indicates miR-16 to be the most abundant and miR-497 the least abundant cardiac miR-15 family members.

B. Quantitative analysis of the different miR-15 family members in fibroblasts or cardiomyocytes indicates that the relative abundance of the different members is comparable for fibroblasts and myocytes with miR-16 being the most abundant and miR-497 expression being lowest.

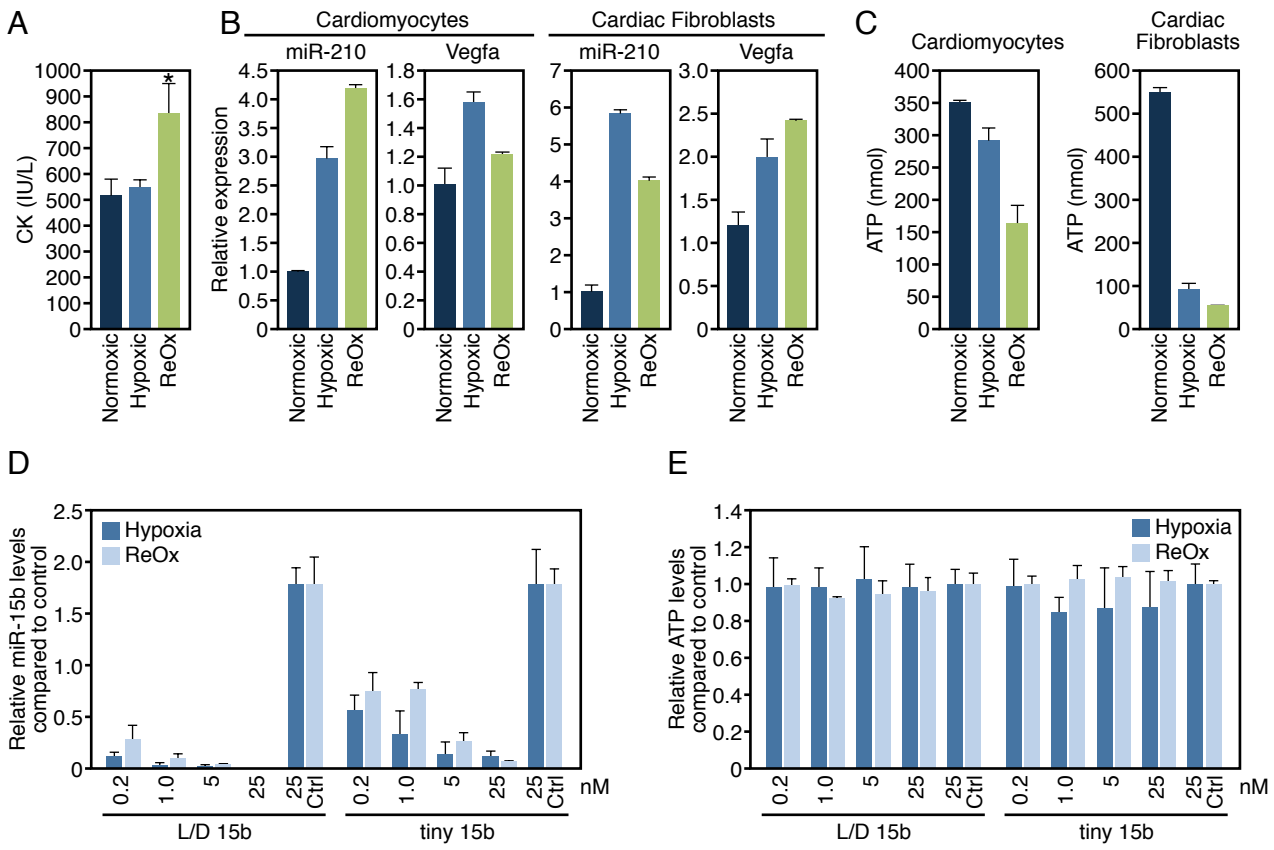

Online figure IV. Effects of antimiR-15 treatment on cardiomyocytes and fibroblast under hypoxic conditions.

A. Increased levels of creatine kinase release in neonatal cardiomyocytes indicate cell injury in response to hypoxia and hypoxia/reoxygenation. (* $p<0.05$ vs. normoxia by ANOVA).

B. Realtime PCR analysis of miR-210 and Vegfa expression confirms hypoxia in both cardiomyocytes and fibroblasts.

C. ATP measurements in both cardiomyocytes and fibroblasts indicate a reduction in cell survival in response to hypoxia and hypoxia with subsequent reoxygenation.

D. Realtime PCR analysis shows a dose-dependent decrease in miR-15b levels in response to both L/D 15b and tiny 15b, while the control chemistries have no effect.

E. miR-15 inhibition has no effect on fibroblast survival during hypoxia or hypoxia with subsequent reoxygenation.

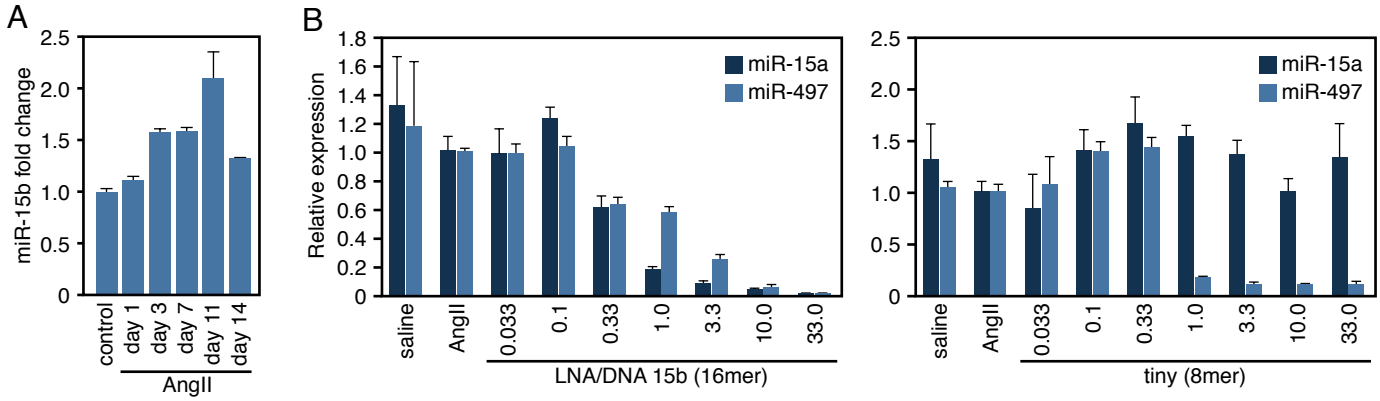

Online figure V. Angiotensin II treatment increases cardiac levels of miR-15b in mice.

A. Angiotensin II administration significantly induces cardiac levels of miR-15b starting 3 days after treatment.

B. Realtime PCR analysis shows that tiny regulates miR-497 robustly at 1 mg/kg in vivo, however, tiny has no effect on miR-15a levels. Additionally, L/D 15b shows dose-dependent inhibition of both miR-15a and miR-497.

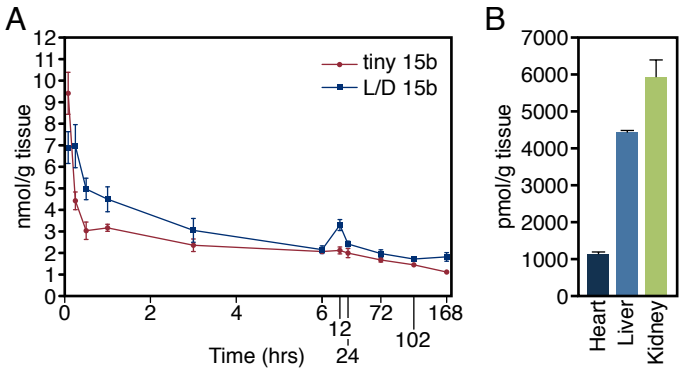

Online figure VI. Biodistrubition data for tiny 15b in murine tissues.

A. Cardiac detection of 33 mg/kg of L/D 15b or an equivalent molar dose of tiny 15b shows a high level of detection immediately after injection which stabilizes 6 hours after administration. The antimiRs remain present till at least a week after administration.

B. Tiny 15b can be detected in heart, liver and kidney 1 week after i.v. delivery of 33 mg/kg.

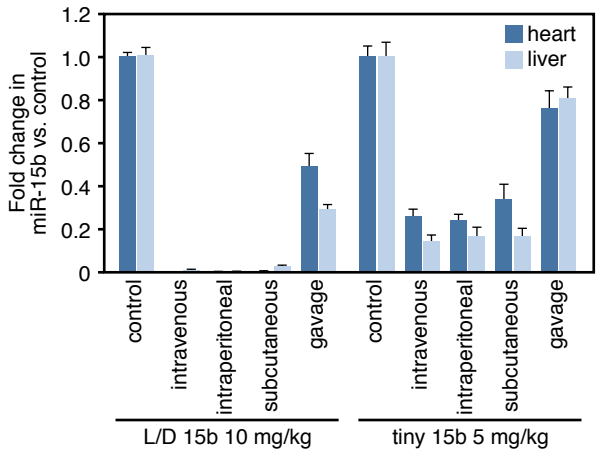

Online figure VII. Cardiac inhibition in response to antimiR delivery via different routes of administration.
Realtime PCR analysis 4 days after intravenous administration of increasing doses of L/D 15b or tiny 15b indicates potent silencing of cardiac miR-15b.

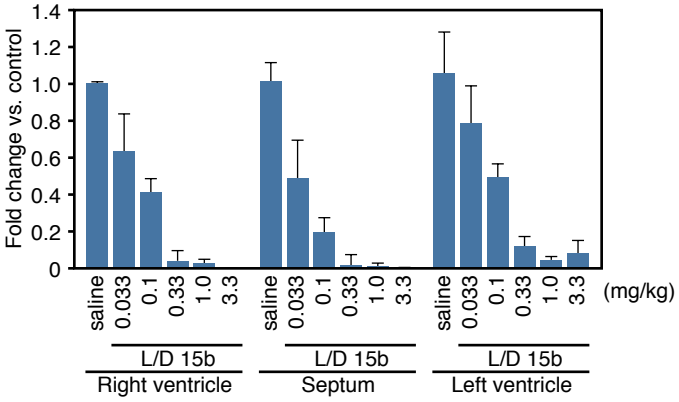

Online figure VIII. miR-15b inhibition across the different cardiac regions of a porcine heart.
Realtime PCR demonstrates a similar degree of miR-15b inhibition in both ventricles with L/D 15b 4 days post treatment in the pig.

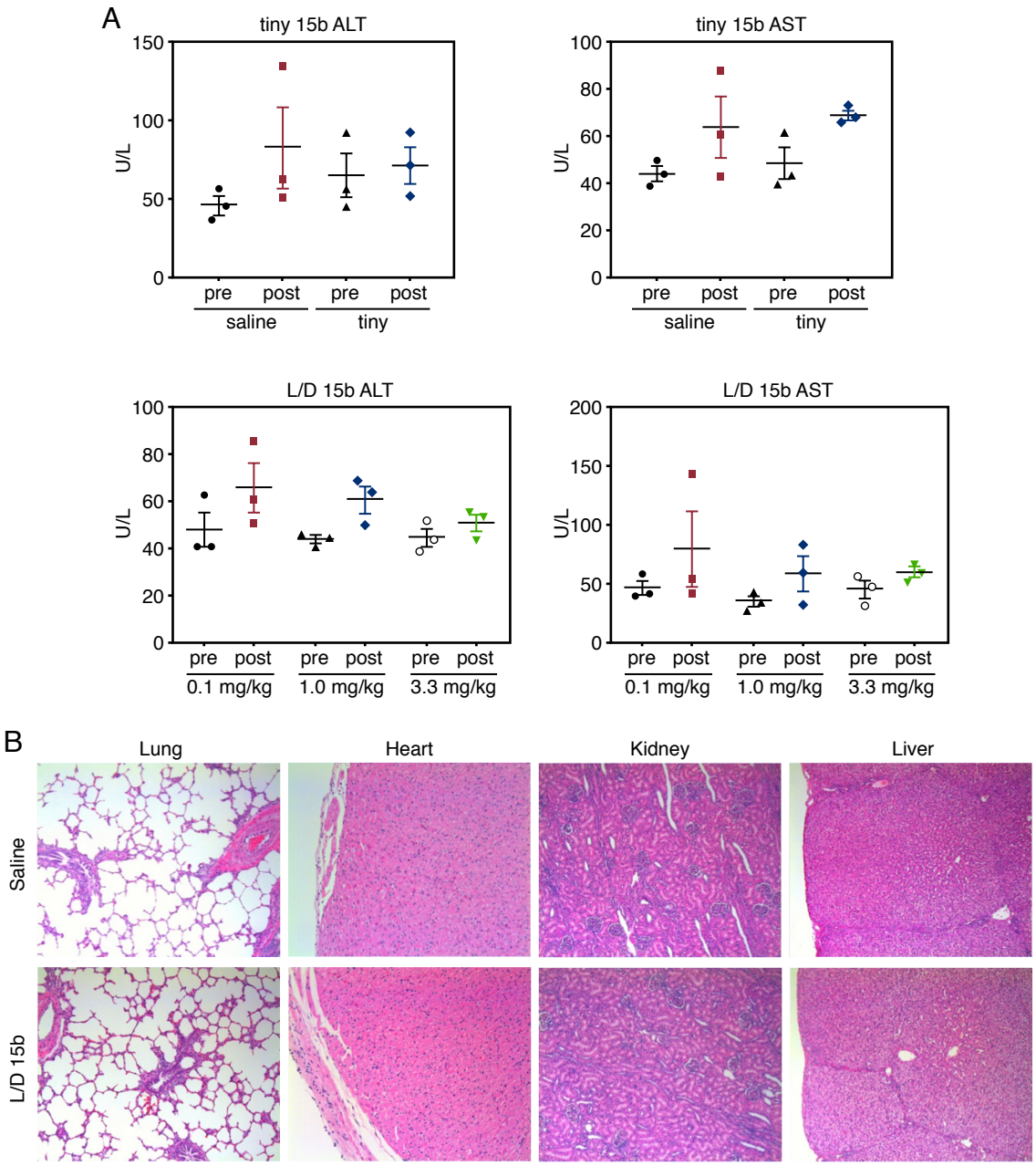

Online figure IX. Effects of miR-15b antimiRs on serum AST and ALT levels in the pig.

A. Serum levels pre-dosing (pre) and 4 days post dosing (post) were assessed in saline treated, tiny 15b treated (5.18 mg/kg) and 0.1, 1.0 and 3.33 mg/kg of L/D 15b. Effects of antimiR treatment were not different than saline and no dose response was observed in the L/D 15b treated animals.

B. Histolopathologic examination of H&E stained tissues from lung, heart, kidney and liver revealed minimal pathology with no relationship to L/D 15b treatment. Images 4 days post L/D 15b treatment in the pig.

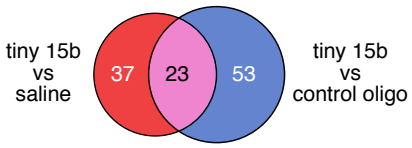

ACSL4	MED1
ARRDC4	MTMR3
CDC37L1	PAM
CNOT6L	PCDH17
DDX3X	PCMT1
DNAJA2	PDK4
EIF4E	RNF125
FKBP5	SGK1
IRS2	SMAD5
KIF1B	SOX5
KPNA3	WDR32
LPHN1	

Online figure X.
Venn diagram showing that 23 Target-Scan predicted genes upregulated by microarray analysis based on tiny vs. saline treatment and tiny vs. control oligo treatment (≥ 1.5-fold). Tiny vs. saline treatment revealed 37 transcripts. Tiny vs. control oligo treatment revealed 53 transcripts. The 23 transcripts that are in common between the two comparisons are listed.